Progress in Additive Manufacturing (2025) 10:6007–6028
https://doi.org/10.1007/s40964-025-00949-1

FULL RESEARCH ARTICLE

Green electropolishing treatment of Ti6Al4V EBM parts: effect on morphology and corrosion resistance

A. Acquesta[1] · **F. Desiderio**[1] · **T. Monetta**[1]

Received: 18 June 2024 / Accepted: 31 December 2024 / Published online: 22 January 2025

Abstract
The surface finish of additively manufactured (AM) parts is an important drawback of the new technologies. High roughness value could trigger corrosion phenomena and cracks, decreasing mechanical properties. Thus, post-processing treatments able to significantly reduce surface roughness are needed. This work aimed to study the effect on morphology and corrosion resistance of Ti6Al4V cylindrical parts produced by Electron Beam Melting technology and post finished with an environmentally friendly electropolishing (EP) treatment. An anodic levelling and brightening of the surface have been obtained modifying the treatment duration time. Morphological, metallographic and crystallographic analyses were performed. The corrosion behaviour was tested by potentiodynamic polarisation technique and electrochemical impedance spectroscopy analysis in a 0.6 M NaCl aqueous solution. A significant modification of the surface morphology was obtained after the EP treatment. A smoothing of the surface reduced the high peaks, but an *orange-peel* skin aspect was yet to show. The complete brightening of the surface has allowed to level the peaks and valleys. The electrochemical measurements revealed an important improvement of the corrosion resistance of the samples electropolished compared to the untreated and wrought samples, used as benchmark.

Keywords Electropolishing · Green surface treatment · Additive manufacturing · Titanium alloy · Roughness · Corrosion · Contour

1 Introduction

Titanium and its alloys are widely used in different industrial fields due to their excellent mechanical properties and corrosion resistance [1]. On the other hand, the conventional machining and surface polishing processes of these alloys are very expensive and time-consuming [2]. In addition, their high oxygen reactivity often requires working in a controlled atmosphere [3]. Based on the powder's overlay, the new manufacturing technology could be the turning point of the titanium manufacturing process. Additive manufacturing (AM) technologies, which differ mainly in the energy source used to build the part, whether it is a laser (selective laser melting, SLM) or an electron beam melting (EBM), allow producing unique, customised and complex shape parts [4]. However, the industrial and academic fields are still studying AM process optimisation since the surface finish and the residual porosity are the main blemishes [5–7]. The former is due to un-melted or partially melted particles attached to the already cooled metal part, deep valleys and visible scan traces, rippling and balling effect in addition to the stairstep one when curved or tilted parts are built [8]. As known, the presence of defects points could trigger corrosion phenomena and cracks, compromising the electrochemical and mechanical properties [9, 10]. Therefore, post-processing treatments are needed for both issues. Generally, thermal treatments such as Hot Isostatic Pressure (HIP) are performed on laser-based additively manufactured components to reduce the porosity [11], whereas mechanical or chemical treatments are carried out to improve surface quality [12–15]. However, the mechanical post-treatments could provide the use of tools, with possible alterations of the surface [16, 17], on the other side the chemical ones employ dangerous reagents such as strong acid [18] and could require a long time of treatment. A green electrochemical polishing (G-ECP) could be an ideal candidate to

✉ A. Acquesta
annalisa.acquesta@unina.it

[1] Department of Chemical Engineering, Materials and Industrial Production, University of Napoli Federico II, Piazzale Tecchio, 80, 80125 Naples, Italy

overcome the alterations involved by the mechanical treatments and avoid toxic reagents used in chemical ones. In addition, the electropolishing treatment allows reducing the roughness to the desired value to obtain a smoothing, which means reducing the roughness at a value higher than 1 µm, or a brightening surface, characterised by a roughness lower than 1 µm [19]. Furthermore, it improves corrosion resistance due to forming an oxide layer on the surface [20].

However, to the best of the author's knowledge, until now few papers investigated the effect on corrosion properties of the electropolishing treatment [21–23] carried out on additively manufactured titanium alloy. Among them, one investigated the effect of the electropolishing treatment carried out in an acid-based solution [21], and the others in different eco-friendly electrolytes. In particular, Wu et al. [21] studied the corrosion behaviour in physiological solution and mechanical properties of EBM-produced Ti6Al4V samples electropolished in acid bath by applying different current densities. They highlighting the increase of corrosion phenomena on the electropolished samples treated at a current density value higher than about 300 mA/cm^2. Tsoeunyane et al. [22] compared the results of SLM-produced titanium alloy mechanically polished or electropolished using one acid or two acid-free eletrolytes at a current density value of 200 mA/cm^2. The electrochemical characterization, very roughly investigated, showed the better corrosion resistance of the samples electropolished in one of the two acid-free solutions compared to the mechanically polished. Zhang et al. [23] evaluated the corrosion properties of SLM-produced titanium alloy samples electropolished in an eco-friendly solution, changing the amount of magnesium chloride (from 0.1 to 0.5 M) added to ethylene glycol and deionized water, that composed it. The authors showed the higher corrosion resistance carried out in Ringer's solution of samples electropolished in the solution composed of 0.4 M of magnesium chloride, which involved the lowest roughness. None of these papers investigated the additive manufactured titanium alloy parts after an electropolishing treatment: (i) the corrosion properties in the 3.5% sodium chloride aqueous and (ii) the evolution of the corrosion properties in the time. A relevant aspect is that the researchers have not taken into account also the fact that the objects produced by the additive manufacturing samples are printed starting or finishing their surface with a so-called contour layer [24]. Thus, the electropolishing treatment could dissolve the samples until to expose a surface belong or not the contour layer. Generally, the contour layer is printed by applying the contour-core strategy, where different processing parameters are used for the bulk and perimeter. As a result, the microstructure of it could be different from the bulk, as reported by [25].

Thus, the aim of this paper was to study the corrosion properties and morphology of Ti6Al4V EBM-additively manufactured parts after a green electropolishing treatment carried out at different times to obtain two different roughness levels. In particular, a smooth or a bright level was obtained. The first is by a slight partial dissolution of the contour, the latter by complete dissolution of the contour, enough to expose the bulk of the sample. Thus, the corrosion properties of the electropolished samples were correlated with the morphological, metallographic and crystallographic results by comparing them with that obtained from the untreated, bulk and wrought counterpart; the latter was used as a benchmark.

2 Materials and methods

The additive-manufactured samples were produced using Ti6Al4V powders, whose composition is reported in Table 1.

The components were printed by Electron Beam Melting technology (EBM), whose process parameters are reported in a previous paper [26]. In particular, the powders size was in the range of 45–106 µm (94% of the mass), resulted in the range of 53–75 µm for 62.1% of the mass. A layer thickness of 50 µm was adopted. The samples were printed with a contour of 1 mm, to reduce the roughness, with process parameters covered by copyright, as other of them. Thus, the contour becomes the surface to be electropolished.

The samples were made according to a cylindrical geometry (0.8 cm in diameter and height 8 cm). Figure 1 shows the building direction adopted.

The samples were cut along XY and YZ planes, orthogonal to each other, to study their microstructures. They were embedded in a conductive resin leaving areas of 1 cm^2. A polishing instrument (Tegramin20, Struers) was used for the metallographic preparation by following the ASTM E3-11(2017) standard: grinding with SiC papers P220 and P400, polishing with 9 µm diamond suspension and colloidal silica suspension. Subsequently, a Kroll solution, composed of 2 mL hydrofluoric acid, 5 mL nitric acid, and 100 mL distilled water, was poured on the sample at room temperature for about 20 s. Before the observations, all samples were ultrasonically rinsed in acetone, ethanol and distilled water for 10 min, respectively.

Table 1 Chemical composition of Ti6Al4V powders used to build the AM parts

Al (%)	V (%)	Fe (%)	O (%)	N(%)	H (%)	C (%)	Ti (%)
6,40	4,12	0,18	0,14	0,01	0,003	0,01	Balance

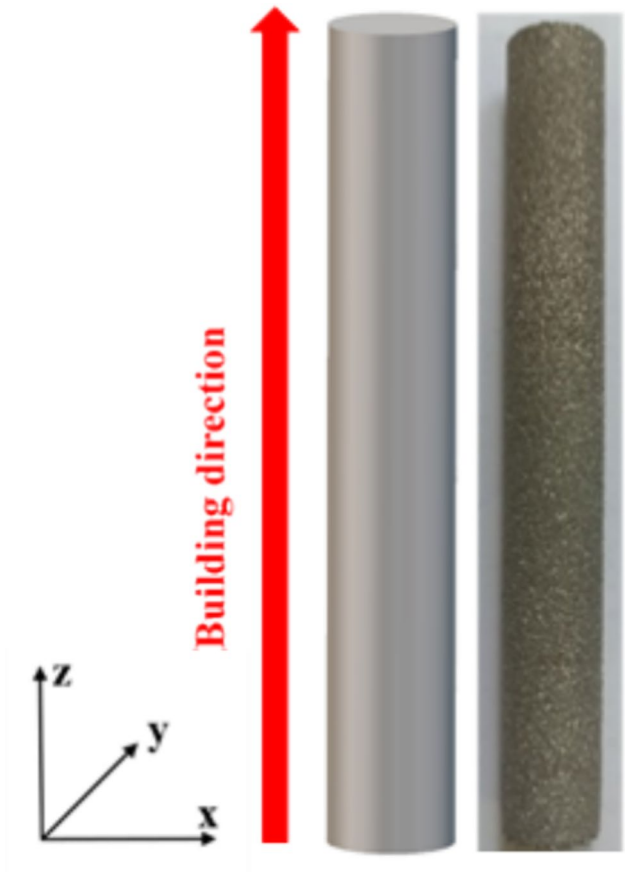

Fig. 1 Building direction adopted to produce cylindrical Ti6Al4V EBM-manufactured parts

2.1 Green electrochemical polishing treatment

The samples were electropolished in the green solution, composed of ethylene glycol (> 99%), 0.5 M of NaCl and 10% vol. of ethanol, using the set-up cell depicted in a previous paper [26], for a duration time to obtain a smooth or a completely bright surface, 60 min or 320 min, respectively. Briefly, the cell consisted of the anodic electrode (the cylindrical titanium sample) and a hollow cylindrical cathodic electrode made of the same material as the anode. The cell was immersed in the green solution at room temperature, controlled by a thermal bath, stirred by means of a magnetic stirrer bar. The parameters fixed for the G-ECP treatment are reported in Table 2.

The tested specimens have been identified throughout the paper using the abbreviations shown in Table 3.

2.2 Characterisation methods

Morphological and microstructural analyses were performed using a confocal laser scanning microscope (Lext 5100, Evident Olympus, Milano) and Scanning Electrone Microscope (SEM, Zeiss Evo 10, Milano) equipped with an Energy Dispersive X-ray (EDX) probe employed for chemical analysis. Crystallographic measurements (XRD) were carried out in Bragg–Brentano geometry with a scanning range of 20 to 80° on Ti6Al4V wrought, as-built EBM, EBm-bulk XY and EBM-bulk YZ samples. The gracing incident X-ray diffraction (GI-XRD) analysis (PANalytical X'Pert PRO, Milano) with a scanning range of 20 to 60° has been used to investigate the crystallographic nature of the film grown on the electropolished samples surface. Roughness measurements have been performed by the confocal microscope previously reported. Electrochemical characterisations were performed using the classical electrochemical cell. The EBM samples were linked to the working electrode, a platinum cylindrical mesh was used as a counter-electrode, and a saturated calomel electrode (SCE) was employed as the reference electrode. In particular, to test the electrochemical behaviour of the as-built and electropolished surface a cylindrical area delimited by two o-rings previously glued, and 1 cm distanced to have a nominal area of 3.14 cm^2 has been selected on the samples (see Fig. 2). Since the electropolishing treatments performed for a long time remove the as-built surface, revealing the bulk material, for comparison the bulk's corrosion properties were investigated by sectioning the samples in the XY and YZ planes orthogonal to each other, electrically connecting with a copper wire passing through a glass tube and embedding in an epoxy resin. Then, they were mechanically polished following the same steps of the metallographic preparation abovementioned.

The corrosion properties were tested in a naturally aerated 0,6 M sodium chloride aqueous solution at room temperature. The open circuit potential (OCP) was initially recorded. A range from − 10 mV to + 3000 mV vs OCP was recorded during the potentiodynamic polarisation test, with a rate of 0.166 mV/s, using a potentiostat (Interface1000, Gamry, USA). The electrochemical impedance spectroscopy analyses were performed for long immersion times in the test solution (0, 1, 2, 4, 7, and 14 days) in the range frequency of 10^5–0.02 Hz, applying a sinusoidal signal of 5 mV vs OCP, with 10 points per frequency decade. Equivalent electric circuits were employed to fit the EIS data using Zview software. Measurements were repeated three times to guarantee repeatability. The curves reported represent the average value of the three measurements.

Table 2 EP treatment parameters applied for electropolishing the samples

Parameters	Values
Applied voltage	25 V
Time	60 min/320 min
Stir rate	1150 rpm

Table 3 Abbreviation adopted to indicate the sampless

	Specimens	Abbreviations
Surface	Ti64 EBM printed and characterised as-is	as-built EBM
EP Surface	Ti64 EBM printed electropolished to obtain a smooth surface (Sa > 1 μm)	EP-EBM-smooth
	Ti64 EBM printed electropolished to obtain a bright surface (Sa ≤ 1 μm)	EP-EBM-bright
Bulk	Ti64 EBM printed, cut in the XY plane, lapped and kept in the air	EBM-bulk XY
	Ti64 EBM printed, cut in the YZ plane, lapped and kept in the air	EBM-bulk YZ
Benchmark	Ti64 traditionally produced, lapped and kept in the air	Ti-6Al-4 V wrought

Fig. 2 Area selected to perform the electrochemical characterisation of the as-built sample

3 Results and discussion

3.1 Electropolishing

The identified electropolishing potential of 25 V corresponds to apply a current density lower than 100 mA/cm^2, as recorded during the treatment and depicted in Fig. 3. Generally, the current density applied for this treatment is higher, as reported by Zhang et al. [23] which performed the electropolishing treatment at 500 mA/cm^2. This means clearly a reduction of the time, but simultaneously a higher weight lost, an increase of bath temperature and bubbles generation.

3.2 Morphological analysis

The morphological analysis taken along the building direction by means of the confocal microscope, reported in Fig. 4, revealed the presence of a high number of un-melted or partially melted particles attached to the cooled parts, evident scanning traces, as well as pronounced depressions unevenly distributed on the surface, observable in the blue nuance in Fig. 4b. It's well known that during the additive processes many phenomena could be presented, such as the balling or the rippling effect, related to the surface tension of the melt pool created as the energy beam hits the metal part [27].

Together with the poor surface quality, the porosity is another drawback of additive manufacturing technologies [28]. As observed by [29] different types of pores could occur: (i) microstructural pores, formed in the bulk of the material, (ii) functional pores, open and connected pores caused by debonding, (iii) structural pores, created intentionally to obtain a controlled porous material. In this case, the observations of the bulk allowed noticing the inherent microstructural porosity of the samples, as shown in Fig. 5, which could become sites of fracture nucleation.

Since the electropolishing treatment allows to customise the roughness level, the duration of treatment has been fixed at 60 min and at 320 min. The optical pictures and microscopic observations of samples after the EP treatment are depicted in Fig. 6. The EP-EBM-smooth specimen (Fig. 6a) revealed the absence of particles attached to the substrate, a smoothing of the peaks, but a remained waviness, so-called *orange-peel skin,* is still observable. While the EP-EBM-bright sample (Fig. 6b) shows the complete reduction of roughness to very low values, so much so that the surface has a shiny appearance and the presence of pores, as observed in the bulk of samples (Fig. 5).

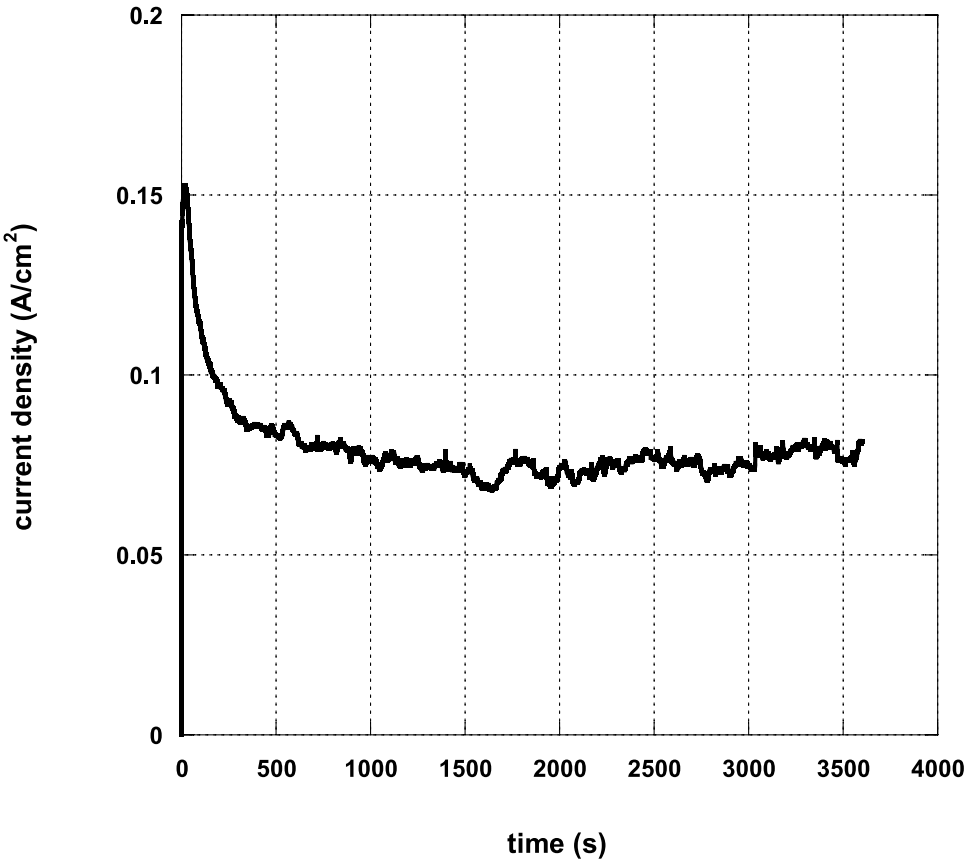

Fig. 3 Chronoamperometric curve of the sample electropolished for 60 min in ethylene glycol-based solution

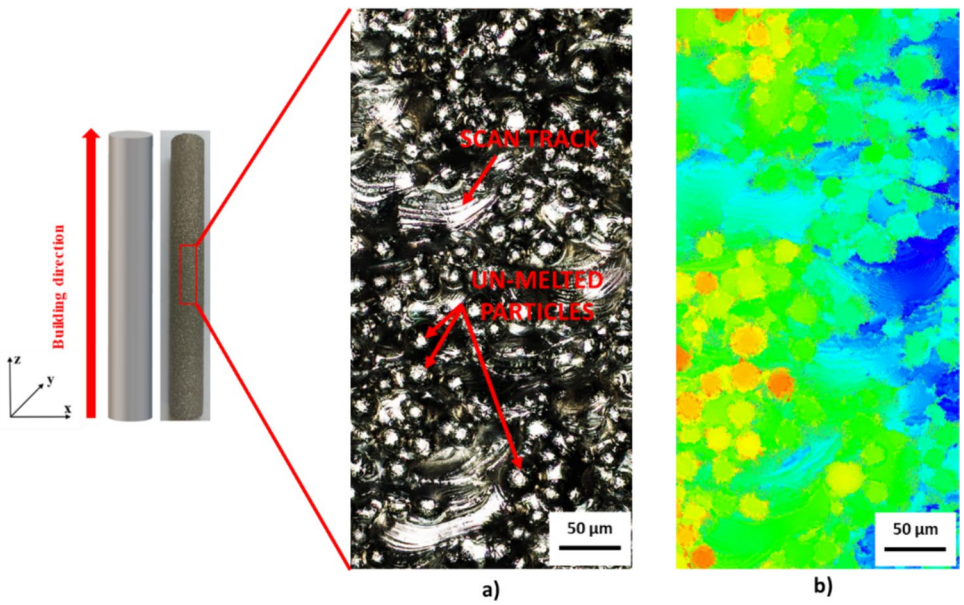

Fig. 4 Microscopic observations of a particular of the as-built EBM sample

From SEM observations and relative chemical analysis, performed by means an EDX probe, it was possible to better observe the high roughness surface of the as-built sample, with several un-melted particles attached on the substrate. Regarding the chemical composition, the EDX spectrum revealed the principal elements of the alloy, i.e. titanium, vanadium and aluminium, in addition to some impurities, as the silicon adsorbed from the air environment. In contrast to [21, 22], a relevant amount of oxygen was detected (Fig. 7).

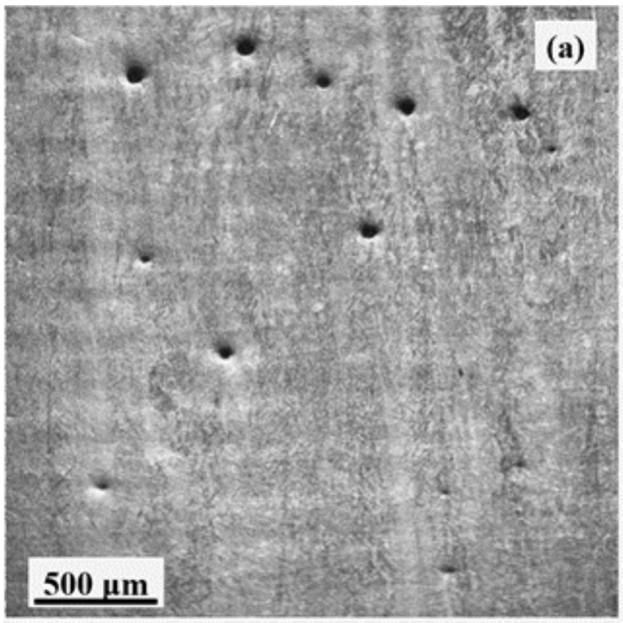

Fig. 5 Pores distribution in the YZ plane

Figure 8 shows the EP-EBM-smooth and EP-EBM-bright samples without the un-melted particles but with, respectively, concave zones and uneven surfaces. On their surface, in addition to the principal elements of alloy, an amount of oxygen was detected, as found by [21–23], smaller than that found on the as-built samples, due to the electrochemical polishing treatment which involved the formation of an oxide layer, called *barrier layer*, thin and amorphous but very compact.

On the other hand, Fig. 9 depicts the SEM and EDX analysis carried out on the bulk samples, in which the oxygen signal was absent, due to their extreme thinness. It's well known that titanium is very reactive with oxygen and a layer immediately growth, but it is on a nanometric scale.

In summary, from morphological point of view, the confocal microscope images combined with the SEM observations highlighted the effective roughness reduction of the as-built samples by means of the proposed green electropolishing treatment.

3.3 Metallographic analysis

First of all, a microstructural analysis was performed on the Ti6Al4V wrought sample. It is possible to note in Fig. 10a the typical microstructure of a conventionally produced and wrought titanium part, composed of equiaxed alpha grains (in white) surrounded by beta phase (in black) [8]. Whereas the classical *lath-type* microstructure, forming alpha phase colonies within the beta phase grains (prior β grain) has been shown by the EBM-bulk XY sample, depicted in Fig. 9b. It is known that the additive manufacturing process, due to its layer-by-layer building strategy, influences the final microstructure, and in turn the mechanical properties. During the printing phase, the titanium alloy is melted at temperatures higher than 1600 °C and, consequently, the β transus (882 °C) is exceeded by going into the stability range of the beta phase. Starting from the latter, by cooling down to room temperature, the stability field of the alpha phase is reached. Depending on the cooling rate, a particular structure is obtained: in the case of components obtained by EBM technology, in which there are no high thermal gradients, initially, the metal solidifies, forming β phase grains oriented along the building direction. As the temperature decreases, the β grain boundaries act as nucleation sites for the alpha phase, obtaining, within the prior β grains, lamellar structures of the alternating alpha and beta phases. If the cooling rate is very high a Widmanstätten microstructure could be formed, characterised by long and acicular plates,

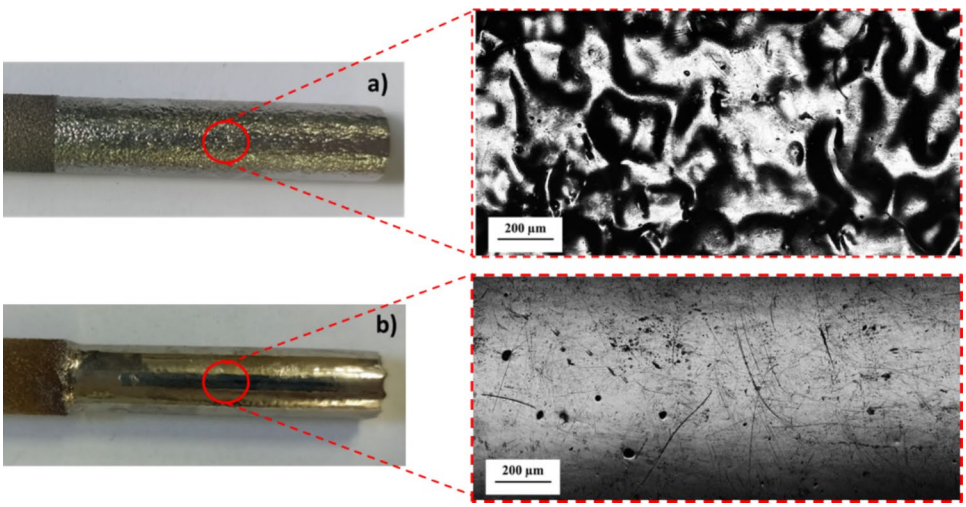

Fig. 6 Optical pictures and microscopic observations of electropolished samples treated to obtain: a) a smooth surface (EP-EBM-smooth) and b) a bright (EP-EBM-bright) surface

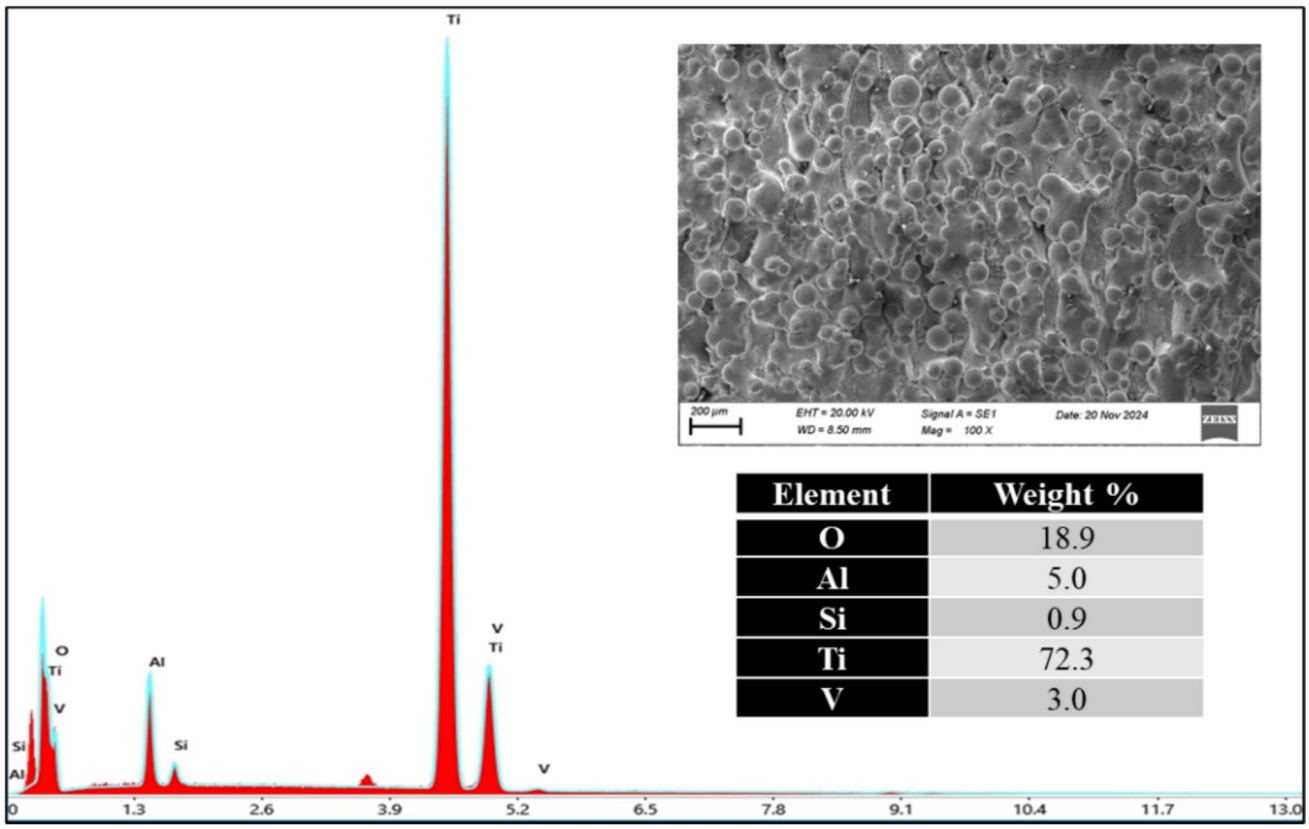

Element	Weight %
O	18.9
Al	5.0
Si	0.9
Ti	72.3
V	3.0

Fig. 7 SEM picture and EDX spectrum of the as built sample

as observed in the horizontal XY plane (Fig. 10b), in which colonies of α phase laths inside large-body primary β-phase grains intertwine with each other as if forming a basket [30]. The microstructural anisotropy characterising the additive manufacturing parts [31] is highlighted in Fig. 10c, in which the YZ plane microstructure is completely different from that seen in the XY plane. In particular, it was possible to observe the layers overlapped along the building direction, their thickness and the epitaxial growth of irregular sizes and shapes β phase grains oriented along the building direction. As abovementioned, the different microstructure along the three spatial directions involves different mechanical properties along each other.

3.4 Crystallographic analysis

From the analysis of the diffractograms, reported in Fig. 11, it is possible to observe, among the characteristic peaks of the bi-phasic titanium alloy Ti6Al4V, according to JCPDS-ICDD 44–1294 card, the peaks of the α phase (hcp) at 2Θ value of 35.09°, 38.42°, 40.17°, 53.00°, 62.95°, 70.66° and 76.22° assigned to the α-phase planes (001), (002), (101), (102), (110), (103) and (112) respectively. According to JCPDS-ICDD 44–1288 card, a single β phase (bcc) peak at 2Θ value of 38.482° assigned to the β-phase plane (110) was observed. The as-built EBM sample has the identical α peaks as the Ti6Al4V traditionally processed sample, however, the β phase peak does not seem to appear, probably due to the manufacturing process, as observed also by [32, 33], which found a β volume phase in the additively manufactured sample approximately 60% lower than that found in the conventionally produced. However, the intensity of the α phase peaks of the EBM bulk YZ sample is higher than the EBM bulk XY one, suggesting an increasing in the grain size along the building direction.

To study the crystallographic structure of the surface after the electropolishing treatment, the analysis was performed by means of the glancing incident X-ray technique (GIXRD), in which a highly collimated beam enters the sample at a very small angle, typically a few degrees or less and allows to investigate the first layers of the surface. In Fig. 12 the spectra of the samples are depicted. On the smooth electropolished sample (EBM-EP-smooth, grey line), in addition to the aforementioned characteristic peaks, others little peaks at 20° and 30° also emerged, indicating the presence on the surface of chemical compounds different from the bulk, because the electropolishing treatment carried out for one hour allowed a good

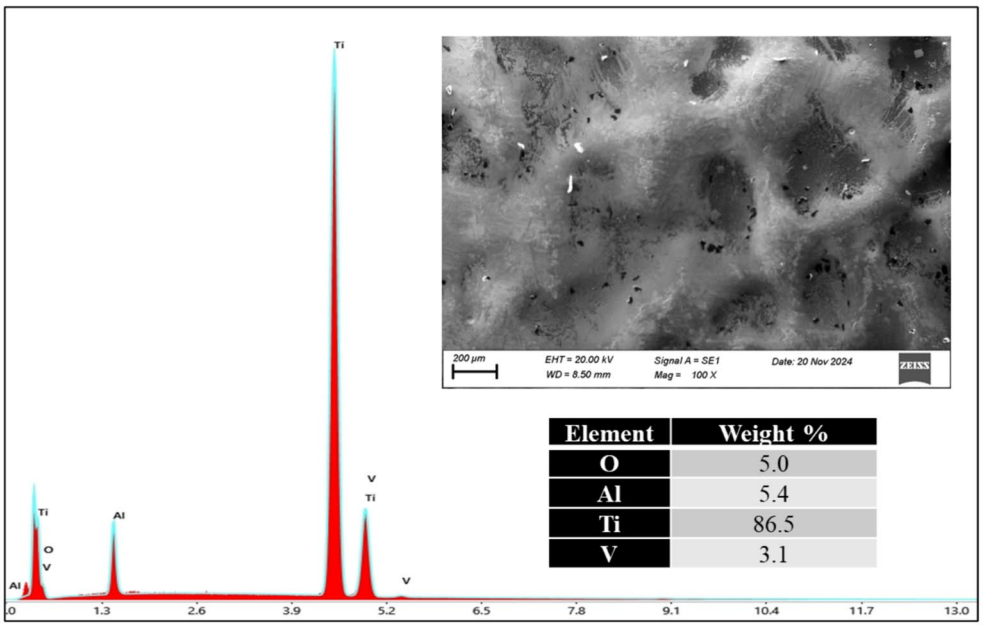

Element	Weight %
O	5.0
Al	5.4
Ti	86.5
V	3.1

a)

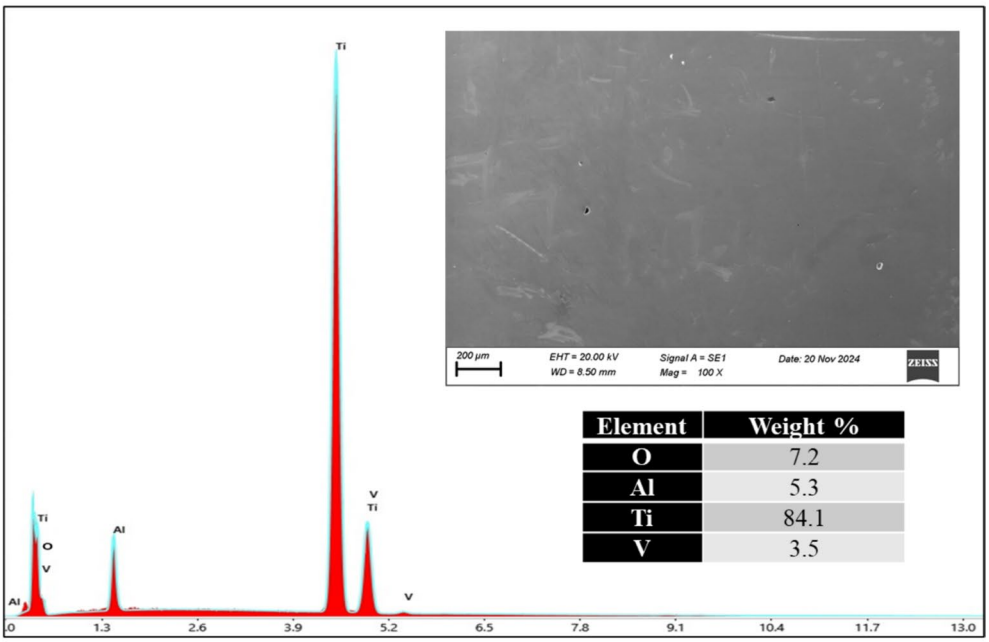

Element	Weight %
O	7.2
Al	5.3
Ti	84.1
V	3.5

b)

Fig. 8 SEM picture and EDX spectrum of the (**a**) EP-EBM-smooth and (**b**) EP-EBM-bright samples

reduction of roughness but the new surface belongs to the contour layer, as below reported. It was printed by using less performing process parameters, so a different microstructure could be formed. In the EP-EBM-bright sample (yellow line), the previous peaks disappeared, and only the α-phase peaks were observed, as for the bulk samples, suggesting that the new surface belongs to the bulk. The lack of oxides peaks, expected in the electropolished samples, was evidently due to their amorphous nature.

3.5 Roughness measurements

The high roughness of the EBM-based manufactured parts is mainly related to the higher dimension of the powders used

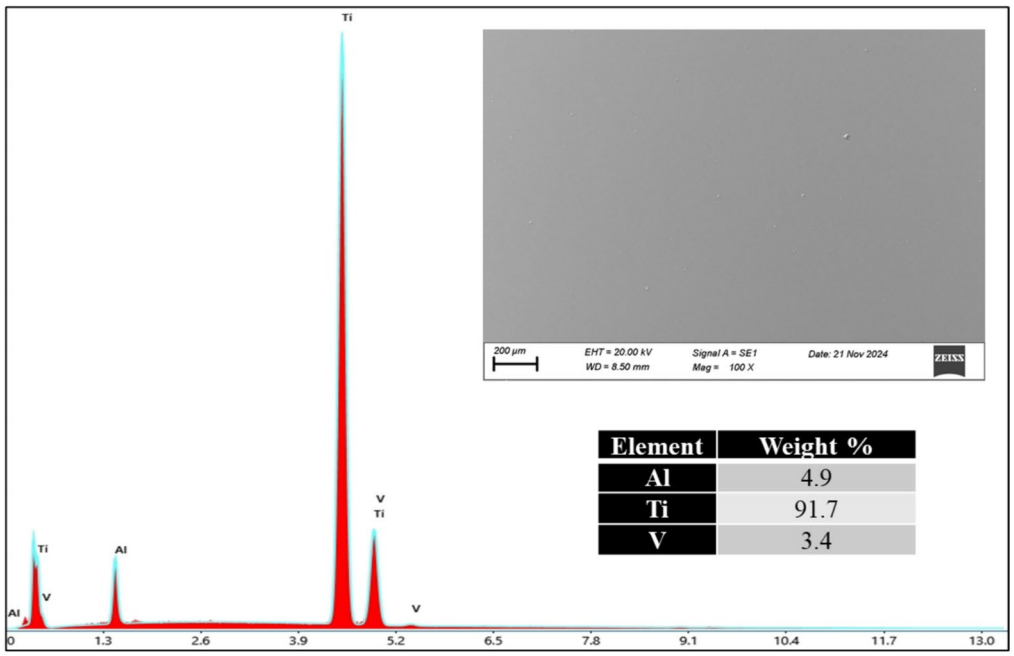

a)

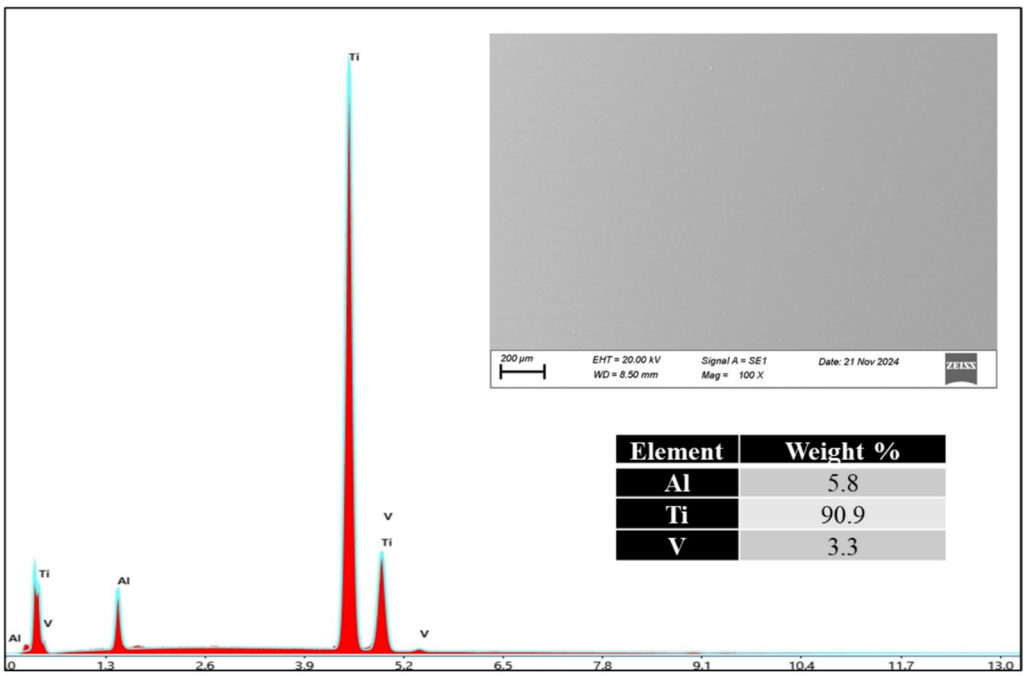

b)

Fig. 9 SEM picture and EDX spectrum of the (**a**) EBM-bulk XY and (**b**) EBM-bulk YZ samples

in the process if compared to those employed in the laser-based technology. The process and the parameters used also affect the surface quality, as before discussed, although the contour layer is printed with different process parameters to optimise it. Although many papers evaluate the roughness parameter R_a to describe the morphology of a surface, it is not sufficient to describe the real morphology; in addition, it does not constitute a discriminating factor in the identification of a particular type of morphology. Indeed, surfaces with the same R_a value could present different aspect [34].

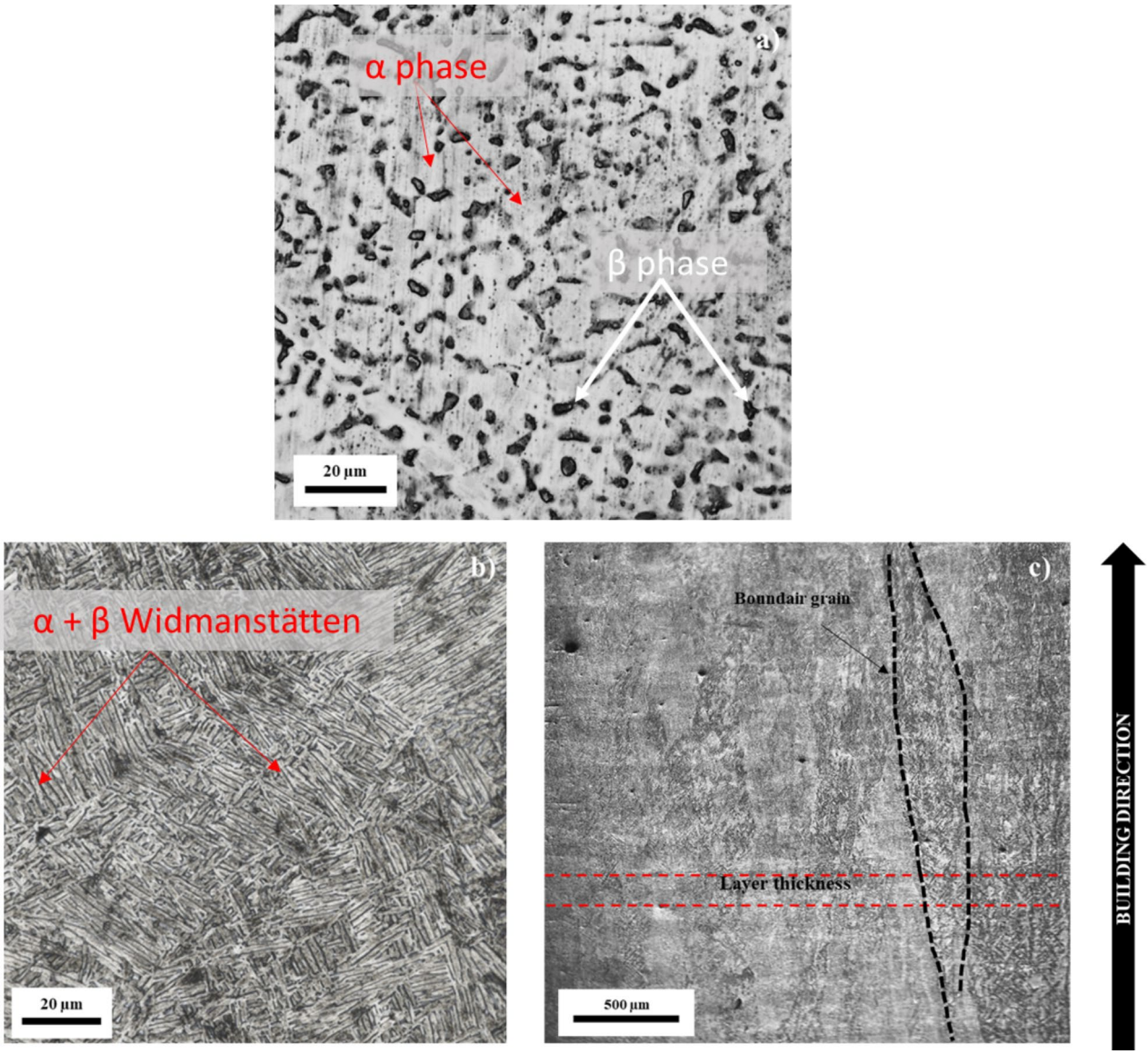

Fig. 10 Microstructures pictures of: **a** Ti6Al4V wrought, **b** EBM-bulk-XY and **c** EBM-bulk-YZ samples

Thus, S_a, which is the extension of the profile roughness to a defined area, together with S_q, the root mean square deviation, kurtosis S_{ku} and skewness S_{sk} parameters have been considered. According to the ISO 4287:2002 standard, the kurtosis parameter, S_{ku}, represents the relation between the height distribution and a Gaussian distribution: if $S_{ku} = 3$ the surface is characterised by peaks and valleys with a gaussian shape; if $S_{ku} > 3$, the surface contains sharp high peaks and valleys while $S_{ku} < 3$ corresponds to an equilateral triangle distribution of peaks and valleys over the surface. The skewness parameter, which can assume positive or negative values, represents the prevalence of peaks or valleys, respectively. In addition, two other surface parameters have been considered: S_{dq} and S_{dr}. The former is the root mean square value of ordinate slope dZ/dx, S_{dq}, and indicates the effectiveness of a treatment aimed at reducing the roughness; the more this value reaches zero, the more flatness of the surface is achieved, the more effective the treatment will be. Whereas S_{dr} is indicative of the ratio between the area developed and that geometrical. In Fig. 13 the 3D roughness acquisitions of the additive manufactured sample before and after the electropolishing treatment were depicted. No similar papers investigated samples with an initial roughness value, Sa, higher than 50 µm, as in this study. In addition, often a profilometer to perform the roughness measurement is used, although the limitation well-known of this kind of instruments, not suitable for measuring highly rough surfaces. Tsoeunyane et al. [22] investigated the reduction of

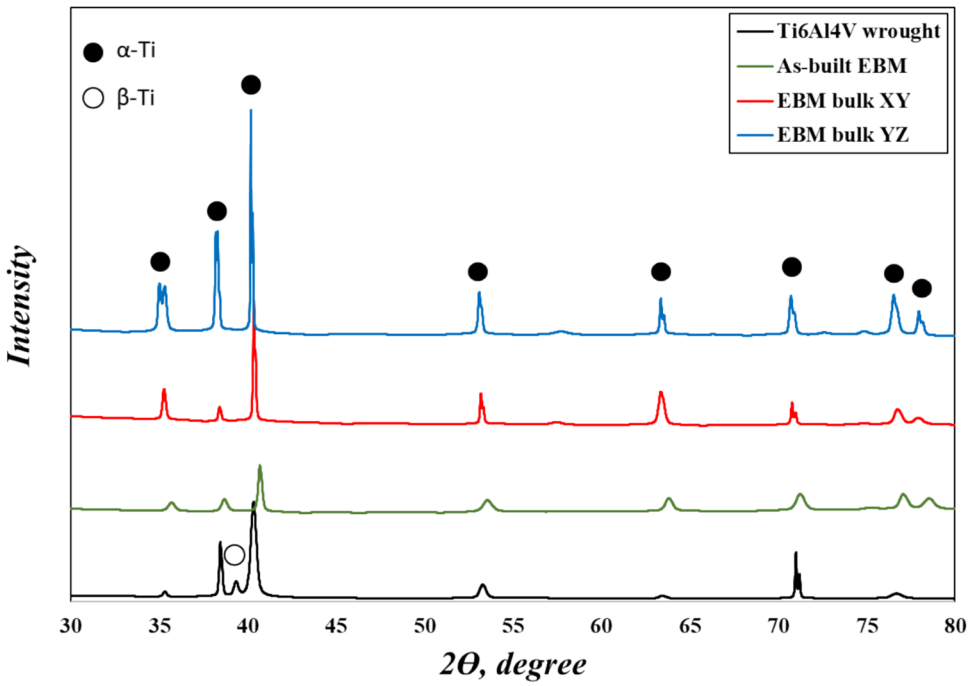

Fig. 11 XRD patterns of Ti6Al4V wrought (black line), EBM-as built (red line), EBM-bulk XY and EBM-bulk YZ (green line) samples

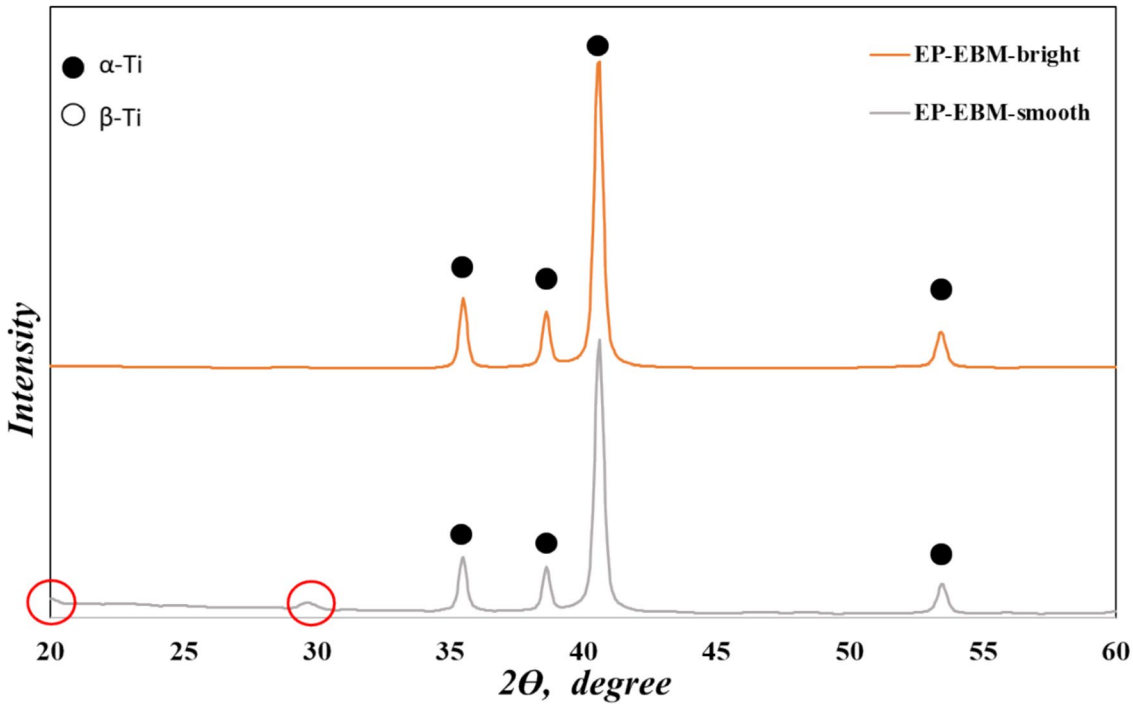

Fig. 12 GIXRD patterns of EP-EBM-smooth (grey line) and EP-EBM-bright (orange line)

the roughness of Ti6Al4V sample obtained by SLM technologies, which presented an initial roughness Ra of about 45 µm. Zhang et al. [23] polished samples characterized by an initial roughness value, Ra, of about 9 µm, while Wu et al. [21] showed an initial roughness value, Ra, of their samples of about 25 µm (Fig. 13).

As possible to observe in Table 4, the Ti6Al4V wrought sample, as expected, presented a very low value of the surface roughness S_a, about 1 µm, a gaussian distribution of the heights with a value of S_{ku} of about 3, a little predominance of valleys, assuming the S_{sk} a negative value, a flat surface as demonstrated by the S_{dq} value of about 1 µm and a developed

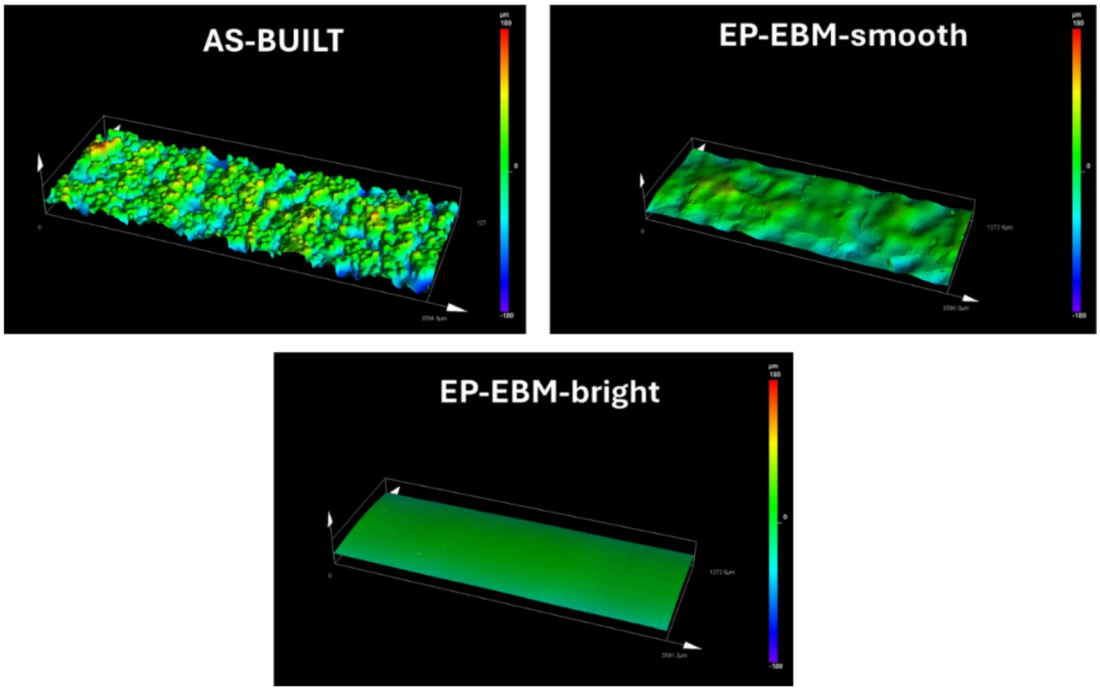

Fig. 13 3D roughness acquisitions of the samples before (As-built) and after (EP-EBM-smooth and EP-EBM-bright) the green electropolishing treatment

Table 4 Surface roughness parameters of as-built and electropolished samples

Sample	Sa(Mm)	Sq(Mm)	Sku	Ssk	Sdq	Sdr (%)
TI6Al4V WROUGHT	1.08 ± 0.02	1.36 ± 0.03	3.19 ± 0.05	− 0.09 ± 0.01	1.22 ± 0. 15	5.08 ± 0.22
AS-BUILT EBM	48.51 ± 0.05	59.88 ± 0.03	2.79 ± 0.04	0.18 ± 0.002	5.33 ± 0.70	184.20 ± 1.30
EP-EBM-SMOOTH	16.52 ± 0.08	21.59 ± 0.02	3.84 ± 0.02	0.23 ± 0.003	1.55 ± 0.03	55.04 ± 0.12
EP-EBM-BRIGHT	1.51 ± 0.04	1.83 ± 0.03	2.54 ± 0.03	− 0.39 ± 0.004	0.16 ± 0.04	1.48 ± 0.08

area of 5%. On the other hand, the as-built samples presented a very high Sa roughness parameter, of about 48 µm. A value of about 3 for the S_{ku} parameter revealed a Gaussian distribution of the heights, whereas a positive value of S_{sk} indicated a predominance of peaks. When the electropolishing treatment was performed for 60 min a smoothing of the surface was obtained, by reducing S_a of about 65%. The smoothing effect is revealed by the S_{dq} parameter, which has been reduced from 5,33 ± 0.70 to 1,55 ± 0.03 and by the decrease of the S_{dr} parameter at a value of about 55%. However, a significant reduction of the roughness has been obtained after 320 min of treatment (EP-EBM-Bright sample) reaching a S_a value of 1.51 ± 0.04 µm. The S_{ku} value minor than 3 suggested a modification of the height distribution, whereas the negative value of S_{sk} indicated the predominance of valleys, probably due to the surfacing of porosities. A value close to 0 of the S_{dq} revealed a very flat surface, with little contribution to the developed area, as demonstrated by its low S_{dr} value of about 1,5%.

Zhang et al. [23] starting from a roughness value of about 9 µm, in the optimized condition by applying 500 mA/cm^2 and high stirring for 10 min, reached a roughness reduction of about 88%. Also, Wu et al. [21] showed a roughness reduction of about 80%, using similar condition in terms of current density and stirring, but using an acidic solution and extended the duration time treatment. Tsoeunyane et al. [22] found the highest roughness reduction (of about 80%) in the nontoxic solution, applying 200 mA/cm^2 quickly stirring for 30 min, twice the values set in this investigation. Thus, it is clear that is possible to change the current density or the potential and the duration time treatment to obtain the lowest roughness. If the current density is increased, the treatment time can be shortened, avoiding the oxygen development during treatment, as described by Wu et al. [21] which found pitting phenomena when the current density value was higher than 400 mA/cm^2 obtaining the lowest roughness value, but the worst corrosion resistance behaviour.

3.6 Electrochemical measurements

To evaluate the corrosion resistance conferred by the G-ECP treatment to the parts, potentiodynamic polarisation and electrochemical impedance spectroscopy tests were carried out in a naturally aerated aqueous solution containing 0.6 M of NaCl at room temperature. Furthermore, the electrochemical properties were compared to those shown by the sample obtained by conventional technology and those of bulk, analysing the behaviour in the orthogonal (XY plane) and parallel (YZ plane) planes to the building direction, since the electrochemical polishing can be performed at the desired roughness reduction. In this investigation, the presence of the contour influence the type of surface exposed after the treatment, because for a defined duration time treatment the new surface can belong to the contour or the bulk, thus influencing the electrochemical response, as soon described.

3.7 Potentiodynamic polarisation

Figure 14a shows the potentiodynamic polarisation (PP) curves of the as-built and electropolished samples, in which the current density was reported vs the geometrical area. However, as reported in a previous paper [8], the real area of the as-built sample should be considered since it is significantly higher than the geometrical one due to the high roughness characterising the additively manufactured parts. In this case, using the S_{dr} parameter evaluated in the roughness measurements, was possible to calculate the estimated area of the as-built sample, which was about 12 cm^2. Therefore, the real electrochemical response is reported in Fig. 14b, where a significant shift toward lower current density is exhibited for the as-built EBM sample (green line) and for the EP-EBM-smooth one (grey line). On the other hand, the EP-EBM-bright, EBM-bulk XY and EBM-bulk YZ samples having a roughness comparable with the conventional produced one, remained almost in the same position.

In general, it was possible to observe the classic potentiodynamic curve of a titanium alloy, with a negative corrosion potential, $E_{corr,}$ and an active–passive behaviour, i.e. as the applied potential increases, there is an initial increase in current density (active or activity region), which stops for a certain range of the potential (passive or passivity region) until the so-called trans-passivity potential, E_{pp}, where the current density increases again. From this point on, pitting phenomena begin along with metal degradation. The fundamental corrosion parameters for active–passive metals, in addition to the potential corrosion abovementioned, are the passivity current density, I_{pp}, which is the current density in the range of passivity and the trans-passivity potential, $E_{pp,}$ which means the maximum potential value at which the metals can be used in safe condition. To evaluate the corrosion current density, i_{corr}, in these cases, is needed to record the cathodic branch of the potentiodynamic polarisation curve (in the following graphs the anodic branch was represented), which was not performed in this case because it was not of interest. Looking at the polarisation curves reported in Fig. 14b, it is possible to observe the Ti6Al4V

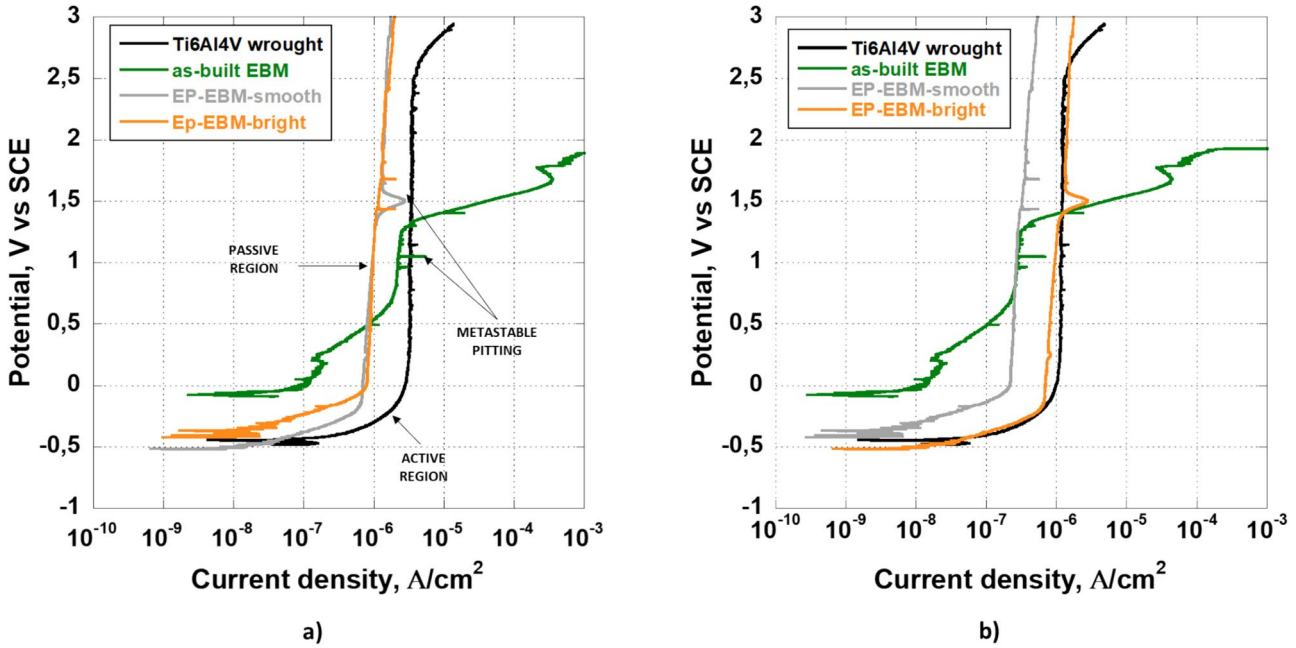

Fig. 14 Potentiodynamic polarisation curves reported taking into account the a) geometrical area and b) estimated area of the conventionally produced, as-built additive manufactured and electropolished samples

wrought curve (black line), characterised by an E_{corr} of about – 0.450 V vs SCE, an active region from E_{corr} to 0 V vs SCE, a passive range from 0 v to 2,5 v vs SCE, a passivity current density of 0.98 ± 0.02 μA·cm^{-2}.

Zhang et al. [23] recorded a potentiodynamic curve in a Ringer's solution for the unpolished sample in which the corrosion potential was of about − 0.5 V vs SCE without recording a passive range but showing a high corrosion current density, being a titanium-based metal. In this study, the as-built EBM sample showed an E_{corr} of about – 0.050 V vs SCE, an active region from the corrosion potential of about 0.05 V to 0.8 vs SCE, followed by a short passive region from 0.8 V to 1.3 V vs SCE, recording a passivity current density of about 0.17 μA/cm^2, in accordance with the literature [7, 20], lower than the wrought sample, due to the higher area. Beyond this potential value, it showed the typical trend of a metal subject to pitting corrosion. The high roughness of the as-built AM components negatively affects the good electrochemical performances of the titanium alloys, triggering corrosion phenomena. This trend was also described by Dai [35] regarding the worst corrosion behaviour of selective laser-melted Ti-6Al-4 V alloy compared to a traditionally produced counterpart.

The curve of the additive-manufactured samples presented the so-called *metastable pitting* points, as also reported by Wu et al. [21], which are current density fluctuations related to the repassivation of pitting points, observed in different active–passive metals. On the other hand, Wu et al. [21] showed a potentiodynamic curve, carried out in Hanks' solution, a kind of simulated body fluid solution, with a corrosion potential of about − 0.250 V vs SCE and a long passive range for the untreated sample, never recorded by other authors due to the very high roughness characterizing the as-built additive manufactured parts. Probably the as-built samples were lapped before the test.

On the other hand, the electropolishing treatment has significantly improved the electrochemical properties of the EBM samples. The partial (smooth) or significant (bright) roughness reduction and the oxide layer formation involves a trend of the PP curves like that shown by the samples obtained using conventional technologies (Ti6Al4V wrought). The beneficial effect of G-ECP treatment could be seen in the extension of the passivity range beyond the values recorded by the conventionally produced counterparts and even a reduction of the passivity current density, of about 1.00 ± 0.04 μA cm^{-2} and 0.25 ± 0.02 μA cm^{-2} for the EP-EBM-bright and EP-EBM-smooth samples, respectively. The presence of a little humpback recorded for the bright samples at 1.5 V against SCE could be related to oxygen reduction, as previously reported [8]. Also, Zhang et al. [23] found a better behaviour of the electropolished samples since they recorded a lower corrosion current density, a well-defined passive range, although they also found a decrease of the corrosion potential and a pitting potential lower than 1 V vs SCE, a singular phenomenon for a titanium alloy. On the other hand, Wu et al. [21] showed an increase of the corrosion potential and a decrease in corrosion current density as the electropolishing treatment was extended, but if the duration time increased a rise of current density they recorded, as detected in this investigation, because of the surfacing of the intrinsic defects such as those reported earlier (Fig. 5) (Fig. 15).

As aforementioned, the electropolishing treatment can remove defined microns of surface, which can be a lesser thickness of the contour layer or so much so as to consume it and exposing practically the bulk, as reported in Fig. 16. It shows that an electropolishing treatment of 60 min (EP-EBM smooth sample in Fig. 16 a) didn't affect the diameter size (equal to the initial diameter of 10 mm) of samples and the final surface belong to the contour layer, whose thickness is detectable by the double inner ring. It means that its microstructure will be different from the bulk, and in turn a possible different electrochemical behaviour could be expected. The different microstructure was revealed also by XRD spectra, in which the EP-EBM-smooth presented additional peaks, compared to the EP-EBM-bright. However, it was very difficult to capture the images of the microstructure due to the circular geometry of the samples. On the other hand, if the treatment is extended the new surface belongs to the bulk, as depicted in Fig. 16b, with a reduction of the cross-section of 1 mm. Thus, from the electrochemical behaviour

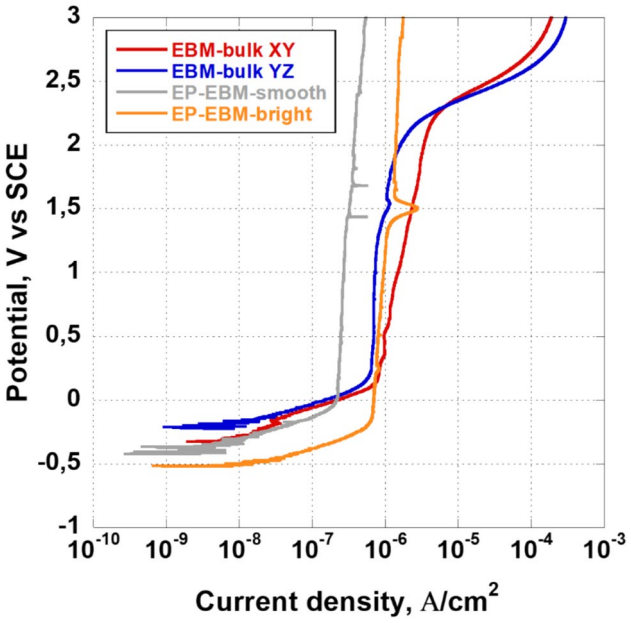

Fig. 15 Comparison of the potentiodynamic polarisation curves taking into account the estimated area of the EBM bulk and electropolished samples

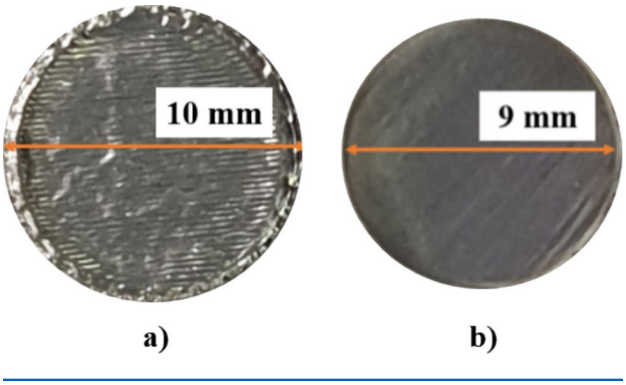

Fig. 16 Cross section of the **a** EP-EBM-smooth and **b** EP-EBM-bright samples

of the EP-EBM-bright one might expect the same electrochemical behaviour of the EBM bulk samples. The surface belonging to the bulk of the EP-EBM-bright samples is evidenced by the same values of current density recorded by this and the EBM bulk samples.

However, as shown in Fig. 15, the curves of the EBM-bulk and electropolished samples presented a different extension of the passive range due to the EP-EBM-bright dissimilar formation mechanism of the oxide layer and for the EP-EBM-smooth both, the different mechanism of the oxide layer and the different microstructure. During the EP treatment, in this case what can be seen during the anodizing process, i.e. the formation through an electrochemical reaction, of a dense and compact oxide layer, albeit thin and amorphous. Nevertheless, it offers a high protection to an aggressive environment. When the metal is exposed to the air at room temperature a thin defective amorphous oxide layer is formed, which can certainly protect the titanium-substrate but until about 2 V vs SCE. The humpback at 1,5 V vs SCE, already detected for the EP-EBM-bright samples, was observed for the EBM YZ sample but it's possible to hypnotize its presence also for the other bulk sample, which presented a slightly current density, tending to hide this bump.

It is interesting to note the anisotropy characterising the additive manufacturing parts, the parallel and orthogonal directions to that of building one [36] presented a little different electrochemical response. Both PP curves show a higher corrosion potential, E_{corr}, than the traditionally manufactured one, indicating a more stable protective oxide film formed on the surface [23], but a slightly lower E_{pp} value of around 2.2 V vs SCE probably due to the different chemical composition distribution [24], in terms of α and β phases distribution, as highlighted by microstructural analysis [37]. The estimated corrosion parameters have been resumed in Table 5.

Table 5 Estimated corrosion parameters considering the real area

Sample	E_{corr} (V vs SCE)	E_{pp} (V vs SCE)	I_{pp} (μA·cm^{-2})
TI6AL4V WROUGHT	− 0.450 ± 0.03	2.5 ± 0.02	0.98 ± 0.02
EBM-BULK XY	− 0.317 ± 0.02	2.3 ± 0.03	1.00 ± 0.05
EBM-BULK YZ	− 0.212 ± 0.04	2.2 ± 0.02	0.95 ± 0.02
AS-BUILT EBM	− 0.072 ± 0.05	1.3 ± 0.03	0.17 ± 0.03
EP_EBM_ SMOOTH	− 0.408 ± 0.02	< 2.5	0.25 ± 0.02
EP_EBM_ BRIGHT	− 0.516 ± 0.04	< 2.5	1.00 ± 0.04

3.8 Electrochemical impedance spectroscopy

The EIS analyses were performed on the EBM samples, keeping them in the aqueous solution test for 14 days. In addition, the EIS measurements of the benchmark sample were performed, whose Bode plots are reported in Fig. 17a, b.

As expected, the titanium conventionally produced sample exposed to a saline solution is characterised by an impedance trend composed of a resistive region in the high-frequency range, followed by a capacitive one in the middle-low frequencies, with an impedance modulus value approaching 10^5 Ω cm^2. The phase angle plot curves recorded a low phase angle value in the high frequency, reaching a value of -80° in the low frequencies, due to the naturally-formed oxide layer on its surface [38], which protects the substrate also in aggressive environments. Increasing immersion time, the impedance modulus and the phase angle plot remained constant, highlighting the high stability of the oxide layer. Also in the EIS analysis, the additively manufactured samples (as-built EBM) seemed to present an EIS response like the Ti6Al4V wrought sample, with a shortly resistive region in the high-frequency range, followed by a capacitive area, recording impedance values in appearance slightly lower than 10^5 Ω cm^2, due to the geometrical rather than real area which has been considered in these graphs. Therefore, the phase angle plot revealed a different behaviour. After the immersion in the test solution in the lowest frequencies a clear and large peak, as if enclosing two constants time, has been detected. After 24 h in the low-frequency domain an improvement of the phase angle has been recorded, which remains constant for all the rest of te observation time. On the other hand, in the high frequency range a slight decrease in capacitance (evident as a translation toward the higher frequencies) was revealed between the first and the last day of immersion. Zhang et al. [22], on the other hand, found a different electrochemical response of the unpolished sample, showing a very low value of impedance modulus at the lowest frequency value, being titanium-based alloy, of about 5×10^3 Ω cm^2 but a similar value of the impedance of the

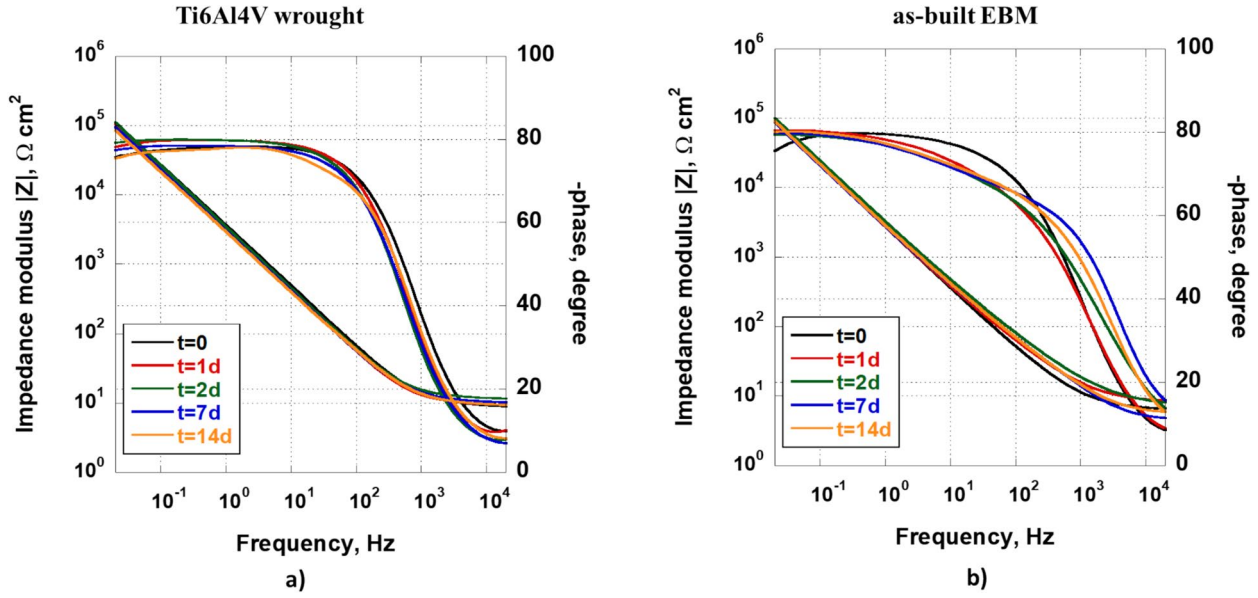

Fig. 17 Bode plots of (**a**)Ti-6Al-4 V wrought and (**b**) as-built EBM samples immersed in a 0,6 M NaCl naturally aerated aqueous solution for 14 days

EP-EBM-bright sample. The Bode plots of the EP-EBM smooth and bright samples are shown in Fig. 18.

A smoothing of the surface involved improving the impedance modulus at low frequencies, reaching a value of 10^5 Ω cm^2, as depicted in Fig. 18a, a reduction of the resistive range in the high-frequency range. After a day of immersion, a decrease and a subsequent increase of the impedance modulus values at the lowest frequency have been recorded for all the whole immersion time. The phase angle plot highlighted a significant modification of the electrochemical response during the immersion time test, suggesting more than one-time constants from the second day of immersion. A translation of the phase maxima versus the high frequency can be seen, suggesting a reduction of the protective properties. It is easy to image that the high variability of behaviour is related to the morphology of the

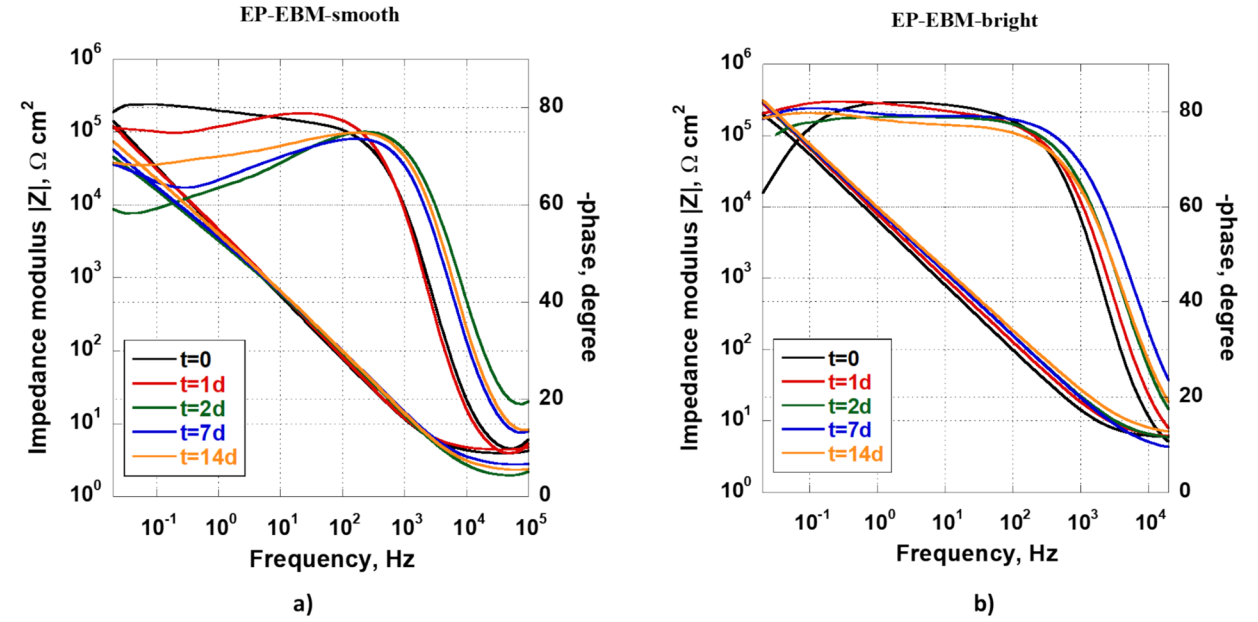

Fig. 18 Bode plots of (**a**) EP-EBM-smooth and (**b**) EP-EBM-bright samples immersed in a 0,6 M NaCl naturally aerated aqueous solution for 14 days

sample under examination, which in this case has a surface with reduced roughness but as seen in the morphological analysis presents a remained waviness, *orange-peel skin*. Probably the concavities that emerge after treatment become stagnation zones where degradation phenomena can easily occur. On the other hand, the brightening of the surface (Fig. 18b) involved a behaviour similar to the wrought sample, highlighting an improvement of the impedance modulus values at low frequencies, which remain constant for all the immersion time, also found by Zhang et al. [22]. The bode-phase plot showed a continuous evolution in the low-frequency domain, from the first to the last day of immersion, suggesting a dissolution and reformation of a passive layer.

Concerning the electrochemical response of the bulk samples, depicted in Fig. 19, evident differences compared to the wrought sample were found. The reason could be due to the higher amount of alpha phase, more nobler than the β phase [35], as shown by XRD analysis in the additive manufactured samples. In addition, a different phase distribution between the orthogonal and parallel planes to that of the building direction could be involved a various electrochemical response. It can be seen the orthogonal plane shows a very short resistive section at high frequencies and a capacitive section at medium–low frequencies. The value of the impedance modulus at 0.02 Hz immediately after immersion in the saline solution is about 3×10^5 Ω cm^2. After 14 days, the modulus reaches a value of 5×10^5 Ω cm^2. The phase angle curves suggest the presence of two constant times, probably due to the oxide thickening, after 24 h of immersion in the test solution. It is possible to check that the behaviour of EBM-bulk XY was similar to the EP-EBM-bright, confirming also by this characterization that the electropolishing treatment performed for a long time exposes a surface belong to the bulk and not yet to the contour layer.

The impedance modulus curves of the EBM-bulk YZ (Fig. 19b) overlapped for all immersion time, suggesting a high stability of the oxide grown on the surface. The impedance modulus records a value of 1×10^6 Ω cm^2 at the lowest frequency immediately after immersion of the sample in the saline solution, according to the literature [35]. It remains constant for the whole immersion time, showing a surface colour variation. Generally, the colouring of the titanium surface indicates the formation of an oxide layer, which protects the metal from aggressive attacks and gives it a high resistance to corrosion.

3.9 Equivalent electric circuits

Equivalent electric circuits were used to model the EIS data. The equivalent electric circuits are networks of electrical elements, as resistor, capacitor, inductor, and so on, used to simulate the electrolyte–electrode interface electrochemical behaviour of a system.

The Ti6Al4V wrought and EP-EBM bright samples were modelled for all immersion time in the test solution with the simple circuit displayed in Fig. 20a [39] composed of the solution resistance R_s, in series to a parallel circuit of CPE_1 and R_1, a constant phase element and a resistor, to represent the double-layer capacitance and the charge transfer resistance, respectively. The constant phase element replaces

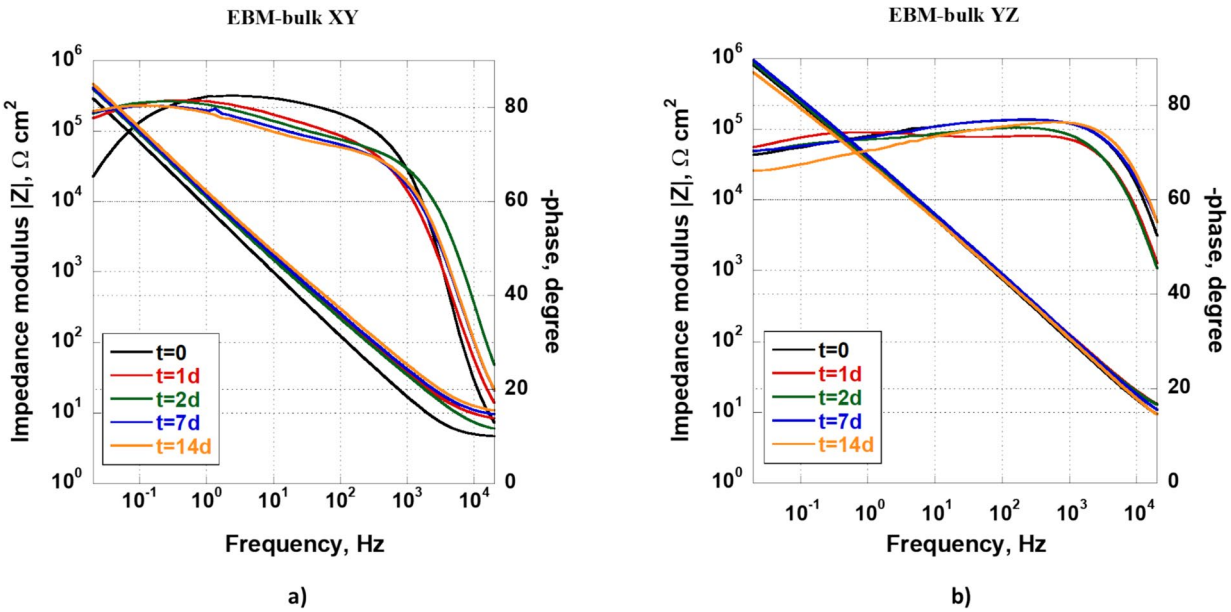

Fig. 19 Bode plots of (**a**) EBM-bulk XY and (**b**) EBM-bulk YZ samples immersed in a 0,6 M NaCl naturally aerated aqueous solution for 14 days

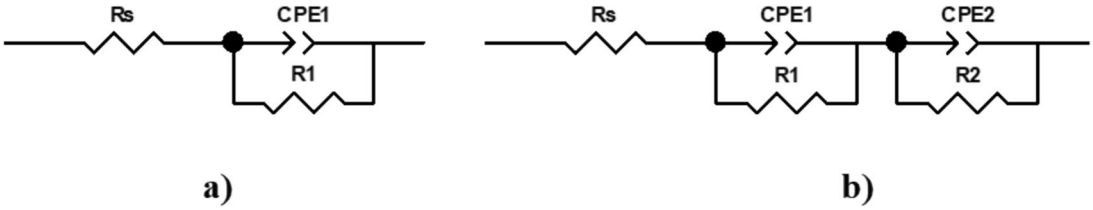

Fig. 20 Equivalent circuit models to fit experimental EIS data of (**a**) Ti6Al4V wrought, EP-EBM-bright and (**b**) As-built, EBM-bulk XY and EBM-bulk YZ samples for all immersion time in the solution test

the capacitance element when the electrode surfaces do not have ideal characteristics. Whereas a good fit for the as-built, EBM-bulk XY and EBM-bulk YZ samples was obtained using the equivalent circuit depicted in Fig. 20b, made of a resistor, representing the solution resistance R_s, in series to two parallels of capacitors and resistors, in series each other [24]. The parallel circuit of CPE_1 and R_1, represents the constant phase element and resistance, respectively, of the film probably produced on the surface; while the CPE_2 and R_2, represent the double-layer capacitance and the charge transfer resistance. Table 6 summarises the results of the fitting EIS data along with the chi-squared value χ^2, which represents the goodness of the fit. A χ^2 lower than 1×10^{-3} indicates a good fit between the experimental and simulated data.

As depicted in Table 6, the wrought sample presented a R_1 value constant for the whole period of immersion, of about 10^6 Ω cm^2. The as-built sample, modelled with the

Table 6 Fitting data results of samples immersed in a 3.5% wt. NaCl naturally aerated aqueous solution for 14 days

Samples	Immersion time	R_s(Ω)	CPE_1 (F cm^{-2})	n	R_1(Ω)	CPE_2 (F cm^{-2})	n	R_2(Ω)	χ^2
Wrought	0	9,1	5,55E-05	0,87	1,72E+06	-	-	-	1,00E-03
	1	9,1	8,53E-05	0,83	5,06E+06	-	-	-	3,00E-03
	2	9,1	6,03E-05	0,89	1,04E+06	-	-	-	2,00E-03
	7	10,5	6,62E-05	0,87	5,31E+06	-	-	-	1,00E-03
	14	9,5	7,09E-05	0,86	3,71E+06	-	-	-	1,00E-03
As-built EBM	0	2,0	1,40E-02	0,50	1,83E+04	2,12E-04	0,892	3,23E+05	9,00E-05
	1	2,6	1,10E-03	0,65	3,40E+04	2,50E-04	0,95	5,43E+05	1,00E-04
	2	1,8	1,74E-03	0,60	6,15E+04	2,61E-04	0,91	9,77E+05	4,69E-05
	7	1,3	4,59E-04	0,72	3,61E+04	3,80E-04	0,99	3,10E+05	6,00E-04
	14	1,7	5,98E-04	0,70	5,10E+04	3,10E-04	0,98	5,05E+05	2,20E-04
EP_EBM_smooth	0	4,8	3,68E-05	0,87	1,55E+07	-	-	-	1,00E-03
	1	5,2	3,66E-05	0,87	1,45E+06	-	-	-	4,00E-03
	2	2,2	3,14E-05	0,86	1,87E+03	4,23E-05	0,57	3,93E+07	5,00E-03
	7	3,2	3,43E-05	0,85	5,50E+03	3,20E-05	0,66	2,90E+07	2,00E-03
	14	2,8	3,02E-05	0,87	3,09E+03	2,10E-05	0,63	5,06E+07	2,00E-03
EP_EBM_bright	0	3,9	4,23E-05	0,91	9,51E+05	-	-	-	1,00E-03
	1	4,1	3,50E-05	0,90	9,36E+06	-	-	-	5,00E-03
	2	3,7	3,21E-05	0,87	2,03E+06	-	-	-	5,00E-04
	7	3,1	3,15E-05	0,88	1,22E+07	-	-	-	1,00E-03
	14	4,5	2,98E-05	0,87	5,30E+07	-	-	-	1,00E-03
EBM-bulk XY	0	3,5	1,12E-04	0,83	7,01E+04	3,64E-05	0,96	5,52E+05	8,62E-04
	1	6,1	4,27E-05	0,81	1,19E+05	3,78E-05	0,99	1,67E+06	1,30E-04
	2	4,0	3,50E-05	0,81	1,74E+05	4,35E-05	0,98	1,51E+06	5,00E-04
	7	6,8	3,08E-05	0,8	2,28E+05	4,52E-05	0,99	1,97E+06	2,70E-04
	14	7,6	2,50E-05	0,81	3,26E+05	4,69E-05	0,98	1,84E+06	7,70E-04
EBM-bulk YZ	0	4,1	2,37E-05	0,85	2,07E+04	6,84E-06	0,86	5,64E+06	1,00E-03
	1	6,5	6,90E-05	0,83	9,65E+04	6,50E-06	0,83	3,57E+07	6,30E-04
	2	6,6	2,59 e-5	0,81	6,58E+04	6,90E-06	0,85	2,61E+07	1,00E-03
	7	4,3	2,02E-05	0,85	2,36E+04	5,87E-06	0,86	7,65E+06	8,30E-04
	14	4,1	1,75E-05	0,84	2,20E+04	8,09E-06	0,85	3,23E+06	2,00E-03

double parallel circuit (Fig. 20b), presented values of R_1 in the order of magnitude of 10^4 Ω cm^2, while one order of magnitude higher was recorded for the R_2 parameter. The electropolishing treatment involved the use of different electrical equivalent circuit in relation to the duration of the treatment. A long duration time (EP-EBM-bright sample), involving a very flat surface, allows using the same equivalent circuit of the wrought sample (Fig. 20a). As the immersion time increases, the value of R_1 also increases, reaching values higher than recorded for the conventionally produced sample, suggesting the formation on its surface of compounds able to boost the corrosion resistance, confirming the result found in the previous characterisation. When electropolishing is carried out long enough to allow for a certain reduction in roughness but not the complete flatness (EP-EBM-smooth sample), a simple circuit (Fig. 21a) can be used to fit the curves for the first day; after that a concatenated double circuit must be used (Fig. 20b). The R_2 values reach value of 10^7 Ω cm^2, but the *n* value of the CPE element is lower than 0.8, indicating a non-ideal capacitive behaviour of the samples. Unexpectedly, a good fit of the additively manufactured bulk samples, either in orthogonal or in parallel direction in relation to the building one, is obtained using the double circuit depicted in Fig. 20b, suggesting the presence of a very stable and thick film on their surface. The EBM-bulk- YZ sample shows lower values of CPE_2 but higher values of R_2 than the XY count part, confirming their little different behaviour, as detected in the potentiodynamic polarisation curves (Fig. 15).

4 Conclusion

The paper aimed to study the effect on morphology and corrosion resistance of EBM-produced Ti6Al4V parts after a green electropolishing performed for different duration times. The important results are summarized in the following.

The electropolishing treatment performed for one hour exposed a surface belongs to the contour layer, whereas an extended duration time treatment exposed a surface belongs to the bulk.

From the crystallographic analysis was possible to observe a spectra of the EP-EBM-bright sample similar to the EBM-Bulk samples, while the presence of two additional little peaks for the EP-EBM-smooth sample, suggests a different crystallographical structure.

The as-built samples presented a very rough surface with a Sa parameter of about 48 µm. The electropolishing treatment performed for 60 min allowed to smooth the surface reducing the Sa parameter of about 65%, the Sdq parameter from 5,33 to 1,55 and the Sdr parameter at a value of about 55%. A significant reduction of the roughness has been obtained after 320 min of treatment reaching a Sa value of about 1,5 µm. A value close to 0 of the Sdq revealed a very flat surface, with a little contribution to the developed area, as demonstrated by its low Sdr value of about 1,5%.

The chemical analysis carried out by means of an EDX probe showed on the electropolished samples, in addition to the principal elements of alloy, an amount of oxygen, accountable to the growth on the surface of an oxide layer during the electropolishing treatment very compact. In contrast, on the EBM-bulk samples the oxygen was not detected due to its very thin thickness.

The high roughness of the as-built AM components negatively affects the good electrochemical performances of the titanium alloys, triggering corrosion phenomena. Whereas the green electropolishing extended the passivity range, characterising the titanium alloys, due to the formation of a thin, compact, but amorphous and so-called barrier layer. The potentiodynamic polarization highlighted a current density of the EP-EBM-bright sample similar to the EBM-bulk samples, and a lower corrosion current density of the EP-EBM-smooth, due to its higher extension sample and a different composition.

Also the electrochemical impedance analysis, carried out for two weeks in a saline solution, showed a different electrochemical response between the electropolished samples, with the response of the EP-EBM-bright very near to that shown by EBM-bulk-XY sample.

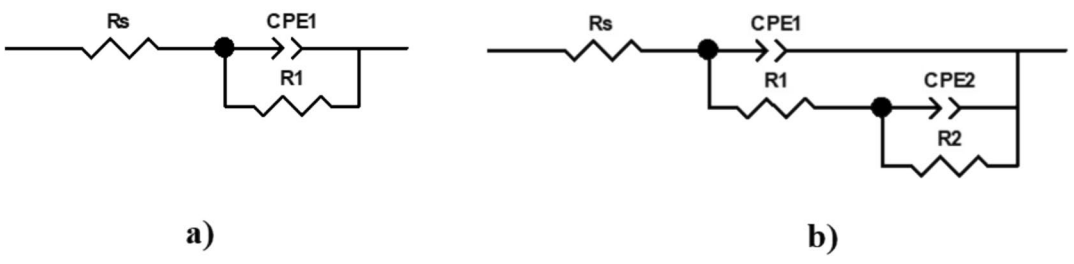

Fig. 21 Equivalent circuit models to fit experimental EIS data of EP-EBM-smooth sample (**a**) at the test beginning or (**b**) after two or seven days of immersion time in the solution test

Thus, the easy and green electropolishing treatment proposed could be a good solution for industrial application as surface treatment for reducing the roughness of the AM parts to a desired level, but also to improve their corrosion resistance. The possibility to use this post-processing treatment in the industrial field for polishing complex shapes, which additive manufacturing technologies can easily produce, must be explored.

Glossary

SLM

It is the acronym of Selective Laser Melting, a kind of additive manufacturing technology which uses a laser for melting a powder bed fluid.

EBM

It is the acronym of Electron Beam Melting, a kind of additive manufacturing technology which uses an electron beam for melting a powder bed fluid.

Ra or Sa

The roughness parameter indicating the arithmetical mean height, evaluated by:

$$R_a = \frac{1}{l}\int_0^l |y(x)|dx$$

Rq or Sq

The roughness parameter indicating the root mean square height, evaluated by:

$$R_q = \sqrt{\frac{1}{l}\int_0^l \{y(x)\}^2 dx}$$

R_{ku} or S_{ku}

The Kurtosis roughness parameter as a measure of the sharpness of the roughness profile, evaluated by:

$$R_{ku} = \frac{1}{R_q^4}\int_{-\infty}^{+\infty} y^4 p(y)dy$$

When $R_{ku} < 3$ the distribution curve is called "platykurtoic" and has relatively few high peaks and low valleys, if $R_{ku} > 3$ the distribution curve is called "leptokurtoic" and has relatively many high and sharp peaks and low valleys.

R_{sk} or S_{sk}

The Swevness roughness parameter as a measure of the symmetry of the roughness profile about the mean line, evaluated by:

$$R_{sk} = \frac{1}{R_q^3}\int_{-\infty}^{+\infty} y^3 p(y)dy$$

A symmetrical height distribution, i.e. with as many peaks as valleys, has zero skewness. Profiles with peaks removed or deep scratches have negative skewness, whereas if the skewness is positive the profile roughness presents filled valleys or high peaks.

Rdq or Sdq

It is a hybrid roughness parameter, a combination of amplitude and spacing. It stands for root mean square of the mean slope of the profile, evaluated as:

$$\Delta_q = \sqrt{\frac{1}{L}\int_0^L \left(\theta(x) - \dot{\theta}\right)^2 dx} \qquad \dot{\theta} = \frac{1}{L}\int_0^L \theta(x)dx$$

Sdr

Developed interfacial area ratio. It is the percentage of surface area that the surface texture adds to an ideally smooth and flat surface of the same cross-sectional area as the measurement region.

OCP

It is the acronym of the Open Circuit Potential, the electrochemical potential of a metal respect to a reference electrode, such as a saturated calomel electrode (SCE), recorded by immersing it in a solution by preventing current from flowing through the circuit.

EIS

It is the acronym of the Electrochemical Impedance Spectroscopy technique, which is performed by applying a low value of tension in an alternating current regime and recording the impedance. It is used to understand the electrochemical mechanism of a system, such as the protective properties of a coating.

Impedance

Frequency-dependent, complex-number proportionality factor, $\Delta U/\Delta I$, between the applied voltage U and the response current I in an electrochemical cell.

Bode plot

Curves of the magnitude of the impedance |Z| and phase angle versus the logarithm of the applied frequency.

Equivalent circuit

An electrical network, consisting of elements such as a resistor, a capacitor and an inductor, which has the same impedance spectrum (i.e. the same response to a perturbation) as the electrochemical system.

Acknowledgements We thank Ing. S. Franchitti and Ing. R. Borrelli, Italian Aerospace Research Centre, for providing the additively manufactured samples used in this research.

Author contributions T. M: Conceptualisation and Supervision; A.A. Conceptualisation. Data curation. Investigation. Methodology. Writing—original draft; F. D data curation.

Funding The research presented in this contribution is partially financed by the Government of Italy Ministry of Education University and Research to the Department of Chemical Engineering, Materials and Industrial Production of the University of Napoli Federico II through the PON R&I 2014–2020 – Axis IV "Education and research for recovery – REACT-EU" Action IV.6 – "Research contracts on Green issues".

Data availability The data presented in this study are available on request from the corresponding author.

References

1. Xu DS, Wang H, Zhang JH et al (2020) Titanium alloys: from properties prediction to performance optimization. In: Andreoni W, Yip S (eds) Handbook of materials modeling: applications: current and emerging materials. Springer, Cham, pp 113–151
2. Niknam SA, Khettabi R, Songmene V (2014) Machinability and machining of titanium alloys: a review. Springer, Berlin, pp 1–30
3. Chen C, Liu L, Zhao R et al (2022) Microstructure evolution and mechanical properties of laser additive manufactured Ti6Al4V alloy under nitrogen-argon reactive atmosphere. Mater Sci Eng A 841:143076. https://doi.org/10.1016/j.msea.2022.143076
4. Korpela M, Riikonen N, Piili H et al (2020) Additive manufacturing—past, present, and the future. In: Collan M, Michelsen K-E (eds) Technical, economic and societal effects of manufacturing 4.0: automation, adaption and manufacturing in finland and beyond. Springer, Cham, pp 17–41
5. Cao L, Li J, Hu J et al (2021) Optimization of surface roughness and dimensional accuracy in LPBF additive manufacturing. Opt Laser Technol 142:107246. https://doi.org/10.1016/j.optlastec.2021.107246
6. Khairallah SA, Anderson AT, Rubenchik A, King WE (2016) Laser powder-bed fusion additive manufacturing: physics of complex melt flow and formation mechanisms of pores, spatter, and denudation zones. Acta Mater 108:36–45. https://doi.org/10.1016/j.actamat.2016.02.014
7. Brennan MC, Keist JS, Palmer TA (2021) Defects in metal additive manufacturing processes. J Mater Eng Perform 30:4808–4818. https://doi.org/10.1007/s11665-021-05919-6
8. Acquesta A, Monetta T (2020) As-built EBM and DMLS Ti-6Al-4V parts: Topography–corrosion resistance relationship in a simulated body fluid. Metals 10:1–15. https://doi.org/10.3390/met10081015
9. du Plessis A, Yadroitsava I, Yadroitsev I (2020) Effects of defects on mechanical properties in metal additive manufacturing: a review focusing on X-ray tomography insights. Mater Des 187:108385. https://doi.org/10.1016/j.matdes.2019.108385
10. Örnek C (2018) Additive manufacturing—A general corrosion perspective. Corros Eng Sci Technol 53:531–535. https://doi.org/10.1080/1478422X.2018.1511327
11. Tammas-Williams S, Withers PJ, Todd I, Prangnell PB (2016) The effectiveness of hot isostatic pressing for closing porosity in titanium parts manufactured by selective electron beam melting. Metall Mater Trans A 47:1939–1946. https://doi.org/10.1007/s11661-016-3429-3
12. Hackel L, Rankin JR, Rubenchik A et al (2018) Laser peening: a tool for additive manufacturing post-processing. Addit Manuf 24:67–75. https://doi.org/10.1016/j.addma.2018.09.013
13. Zhang J, Xiang Toh AY, Wang H et al (2019) Vibration-assisted conformal polishing of additively manufactured structured surface. Proc Inst Mech Eng Part C J Mech Eng Sci 233:4154–4164. https://doi.org/10.1177/0954406218811359
14. Lesyk DA, Dzhemelinskyi VV, Martinez S et al (2021) Surface shot peening post-processing of inconel 718 alloy parts printed by laser powder bed fusion additive manufacturing. J Mater Eng Perform 30:6982–6995. https://doi.org/10.1007/s11665-021-06103-6
15. Scherillo F (2019) Chemical surface finishing of AlSi10Mg components made by additive manufacturing. Manuf Lett 19:5–9. https://doi.org/10.1016/j.mfglet.2018.12.002
16. Denti L, Bassoli E, Gatto A et al (2019) Fatigue life and microstructure of additive manufactured Ti6Al4V after different finishing processes. Mater Sci Eng A 755:1–9. https://doi.org/10.1016/j.msea.2019.03.119
17. Okura Y, Sasaki H, Soyama H (2020) Effect of mechanical properties on fatigue life enhancement of additive manufactured titanium alloy treated by various peening methods. Springer, pp 88–96
18 Bezuidenhout M, Ter Haar G, Becker T et al (2020) The effect of HF-HNO3 chemical polishing on the surface roughness and fatigue life of laser powder bed fusion produced Ti6Al4V. Mater Today Commun. https://doi.org/10.1016/j.mtcomm.2020.101396
19. Sautebin R, Landolt D (1982) Anodic leveling under secondary and tertiary current distribution conditions. J Electrochem Soc 129:946. https://doi.org/10.1149/1.2124071
20. Lee S-J, Lai J-J (2003) The effects of electropolishing (EP) process parameters on corrosion resistance of 316L stainless steel. Proc 6th Asia Pac Conf Mater Process 140:206–210. https://doi.org/10.1016/S0924-0136(03)00785-4
21 Wu Y-C, Kuo C-N, Chung Y-C et al (2019) Effects of electropolishing on mechanical properties and bio-corrosion of Ti6Al4V fabricated by electron beam melting additive manufacturing. Materials. https://doi.org/10.3390/ma12091466
22. Tsoeunyane GM, Mathe N, Tshabalala L, Makhatha ME (2022) Electropolishing of Additively Manufactured Ti-6Al-4V surfaces in nontoxic electrolyte solution. Adv Mater Sci Eng 2022:6987353. https://doi.org/10.1155/2022/6987353
23 Zhang Y, Li J, Che S, Tian Y (2019) Electrochemical polishing of additively manufactured Ti–6Al–4V alloy. Met Mater Int. https://doi.org/10.1007/s12540-019-00556-0

24. Habeeb VVN, Islam R, Chou K (2024) Influence of pre- and post-contouring strategies to downskin sloped surfaces in laser powder-bed fusion (L-PBF) Additive manufacturing. Materials 17:2639. https://doi.org/10.3390/ma17112639
25. Karimi P, Schnur C, Sadeghi E, Andersson XJ (2020) Contour design to improve topographical and microstructural characteristics of Alloy 718 manufactured by electron beam-powder bed fusion technique. Addit Manuf 32:101014. https://doi.org/10.1016/j.addma.2019.101014
26. Acquesta A, Monetta T, Franchitti S et al (2023) Green electrochemical polishing of EBM Ti6Al4V samples with preliminary fatigue results. Int J Adv Manuf Technol. https://doi.org/10.1007/s00170-023-11400-6
27 Acquesta A, Monetta T (2023) Green approach for electropolishing surface treatments of additive manufactured parts: a comprehensive review. Metals. https://doi.org/10.3390/met13050874
28 Ball S, Ghayoor M, Pasebani S, Tabei A (2021) Statistical analysis of porosity and process parameter relationships in metal additive manufacturing. Proc Manuf 53:343–347. https://doi.org/10.1016/j.promfg.2021.06.037
29. Sola A, Nouri A (2019) Microstructural porosity in additive manufacturing: The formation and detection of pores in metal parts fabricated by powder bed fusion. J Adv Manuf Process 1:e10021. https://doi.org/10.1002/amp2.10021
30 Shugurov A (2020) Recovery of scratch grooves in Ti-6Al-4V alloy caused by reversible phase transformations. Metals. https://doi.org/10.3390/met10101332
31. Safdar A, Wei L-Y, Snis A, Lai Z (2012) Evaluation of microstructural development in electron beam melted Ti-6Al-4V. Mater Charact 65:8–15. https://doi.org/10.1016/j.matchar.2011.12.008
32. Zhou L, Deng H, Chen L et al (2021) Morphological effects on the electrochemical dissolution behavior of forged and additive manufactured Ti-6Al-4V alloys in runway deicing fluid. Surf Coat Technol 414:127096. https://doi.org/10.1016/j.surfcoat.2021.127096
33. Huang J-Y, Chang C-H, Wang W-C et al (2020) Systematic evaluation of selective fusion additive manufacturing based on thermal energy source applied in processing of titanium alloy specimens for medical applications. Int J Adv Manuf Technol 109:2421–2429. https://doi.org/10.1007/s00170-020-05797-7
34. Monetta T, Acquesta A, Bellucci F (2014) Evaluation of roughness and electrochemical behavior of titanium in biological environment. Metall Ital 106:13–21
35. Dai N, Zhang L-C, Zhang J et al (2016) Corrosion behavior of selective laser melted Ti-6Al-4V alloy in NaCl solution. Corros Sci 102:484–489. https://doi.org/10.1016/j.corsci.2015.10.041
36. Mazumder S, Pantawane MV, Ho Y-H, Dahotre NB (2020) Spatial response of laser powder bed additively manufactured Ti6Al4V to temperature variation of aqueous electrolyte. Appl Phys A 126:902. https://doi.org/10.1007/s00339-020-04082-4
37. Wang C, Zhu P, Wang F et al (2022) Anisotropy of microstructure and corrosion resistance of 316L stainless steel fabricated by wire and arc additive manufacturing. Corros Sci 206:110549. https://doi.org/10.1016/j.corsci.2022.110549
38. Pan J, Thierry D, Leygraf C (1996) Electrochemical impedance spectroscopy study of the passive oxide film on titanium for implant application. Electrochem Impendance Spectrosc 41:1143–1153. https://doi.org/10.1016/0013-4686(95)00465-3
39. Chen L-Y, Zhang H-Y, Zheng C et al (2021) Corrosion behavior and characteristics of passive films of laser powder bed fusion produced Ti–6Al–4V in dynamic Hank's solution. Mater Des 208:109907. https://doi.org/10.1016/j.matdes.2021.109907